CHAPTER - V

BIOSYNTHESISED NANO METAL OXIDE DISPERSED POLYESTER COMPOSITES AS ENHANCED CORROSION MITIGATORS FOR MILD STEEL IN 0.5 M H_2SO_4

5.1 INTRODUCTION

The catastrophic failures due to corrosion imparting social and economic loss is an undesirable natural process that seems to be unavoidable. This loss is substantially noticed in an aggressive environment which is facilitated by the usage of acid in industrial process like pickling, etching, cleaning of refineries, oil well acidizing and descaling[1-3]. Rating different metals makes the mild steel as one of the prominent low cost material which has broad foot print in construction, power plants, automobiles, desalination units credited with excellent properties which can be moulded according to the desired necessity[4]. As a prompt of practical importance, the strategies to minimise the rate of metal dissolution is seriously investigated by pool of researchers originating from cheapest inhibitors to expensive methodologies. Besides various techniques, addition of corrosion inhibitors[5] holds its everlasting position due to its popularity, inexpensiveness, availability and facile synthesis. To start with, organic inhibitors were chosen as a promising solution which had the capability of minimising the metal loss with a wing of aromaticity, heteroatoms and adsorption sites favouring maximum inhibition efficiency. To site a few, reports given by **Fatma Mohamed Mahgoub *et al.,***[6], **Jamal Abdul Nasser *et al.,***[7], **Yujie Qiang *et al.,***[8], **Ansari *et al.,***[9], **Roland *et al.,***[10] can be reviewed. In recent days quench towards eco-friendly compounds has increased which has diverted researchers to focus on polymeric materials to explore its potential applications. The choice of polymers as corrosion inhibitors has dominated the organic inhibitors due to the following factors[11-13],

(i) Facile synthesis
(ii) Low cost
(iii) Presence of multiple bonding sites
(iv) Complexing ability
(v) Blanketing large surface area

As the emerging technology is in need of new materials, there always exist a crescent tendency to design novel compounds. Developing new materials for successful applications in

pharma, electronics, food processing, cosmetics and so on has paved the way for nano technology resulting in any of the nano forms such as nano particles, nano tubes, fullerenes, graphenes, nano fibres, nano sheets, nano clay and nano whiskers. Concerned with polymers, nano technology plays a vital role where dispersion of nano particles in minimum level could enhance its properties and expand its utilisation in various industrial applications[14]. In specific, metal oxide nanoparticles has been targeted nowadays in current research activities by projecting its valuable presence in biological and medical devices, optoelectronics, energy saving devices, catalysis without which life seems to be inevitable[15]. Polymers blended with metal oxide nano particles overcomes inherent restrictions with a new form termed as nano composites inculcated with interesting properties. Since the awareness of mankind is shifting towards eco friendliness, nano composites synthesised using eco-friendly materials and methods has deserved its position due to its unique properties such as biodegradability, ease of processing, sustainability and valuable physico – mechanical nature.

Transition metal oxides has gained considerable attention due to its low cost, ease of availability and vast applications which has intended us to disperse biosynthesised Zinc oxide (ZnO), copper oxide (CuO) and Tin oxide (SnO) nano metal oxides from Avocado seeds with polymers to explore its support in enhancing its inhibition property in a simple, facile, economical and eco-friendly greener approach.

5.1.1 *Persia Americana* -A potential source

Avocado generally termed as *Persia Americana* or Alligator pears, a native of central Mexico[16] is an important member of Lauraceae family whose seeds a non- edible part has a rich profile of phyto constituents[17]. Industrial processing involved the disposal of seeds until its potential in food and medicine specifically against anticancer, antidiabetics, antidandruff, antichlosterol, hyper tension and pain reducers for snake bites, toothaches were known[18]. This is the turn where avocado seeds got worldwide attention. Aiming towards profitable and eco-friendly environment, in the present work avocado seeds have been chosen primarily to make it effective instead of discarding it as waste and secondarily as a cheap bio active source.

5.1.2 Review of literature

Prior to the detailed discussion of the present work, a glimpse of ideas about the previous work carried out has to be viewed. In regard, research carried out with different nano forms is portrayed below.

The contributions made by CeO_2 towards organic-inorganic hybrid conjucate in its protective performance was studied by **Ubong Eduok *et al.,*** by means of electrochemical and surface analytical techniques. Decreased corrosion current density resulted with increased concentration of CeO_2 which formed a protective layer of inhibitor film on steel surface. Cathodic hydrogen evolution was affected due to the increased amount of CeO_2 concentration. Suitable experimental and theoretical approaches were made to validate the results [19].

In situ chemical oxidative polymerization method was adopted by **Alam *et al.,*** to synthesise hybrid nanocomposite (PPy/GNS/RE^{3+}/DBSA) comprising of pyrrole (Py), graphene nano sheets (GNS), rare earth elements (Nd^{3+}, La^{3+}, Sm^{3+}) and dodecyl benzene sulfonic acid (DBSA). The nano composite characterised by FTIR, XRD, SEM and TEM were chemically deposited on the metal specimens using N-methyl-2-pyrrolidone (NMP) solvent and epoxy resin (10%) as binder. Immersion tests and electrochemical measurements were carried out for the coated specimens in 0.1 M HCl medium. As a supporting evidence, the surface of the coated samples before and after immersion was also investigated[20].

An attempt was made by **Shailesh K. Dhoke *et al.,*** where nano Fe_2O_3 was added to the water borne coating system to study the possible interaction using FT-IR. The nano dispersion within the polymer matrix was evaluated by SEM and AFM techniques. Corrosion and UV resistance, mechanical and optical properties of the coated systems were studied which resulted in enhanced and improved properties[21].

Javidparvar *et al.,* synthesised epoxy composites and evaluated its anticorrosive nature based on electrochemical impedance spectroscopy (EIS). To start with, Fe_3O_4 nano pigments characterised by FESEM, FT-IR and TGA were utilised to prepare triethanolamine (surfactant) based morphologies and finally modified with 3-amino propyl trimethoxy silane (APTMS). The corrosion resistance of the epoxy composites were affected by both surface chemistry and surface morphology of nanopigments[22].

Wonnie Ma Ammar Sh *et al.,* synthesised epoxy resins (nano composites) by varying the composition of nanochitosan (NCH) which was incorporated within the chitosan matrix. NCH as well nano composites were characterised by FT-IR, FESEM and XRD for their surface morphology and their thermal response was analysed by DSC and TGA followed by its optical characterisation by UV-vis spectroscopy. The nanocomposites were coated on the mild steel surface to study its corrosion inhibition performance which resulted in enhanced properties[23].

The protection mechanism rendered by polyaniline nanoparticles (PANs) doped phosphoric acid dispersed within Epoxy–Novolac polymer was investigated by **Ghasem Ebrahimi *et al.,***. Uniform dispersion was confirmed from SEM and TEM analysis

followed by its corrosion resistance evaluation by conductivity, OCP, EIS and Tafel polarisation techniques where the coatings were found to stabilise the potential favouring the formation of surface barrier[24].

Ayman M. Atta *et al.,* synthesised magnetic nanogels in a controllable size at room temperature by adopting free aqueous polymerization. The structural confirmation of the nanogels were carried out by FT-IR, SEM and Tem analysis. The synthesised nanogels were evaluated for its corrosion inhibition towards carbon steel in 1 M HCl by electrochemical measurements, where Tafel analysis revealed mixed type of inhibition. Enhanced inhibition efficiency with concentration and temperature was noticed followed by the best fit with Langmuir adsorption isotherm[25].

Al1050 electrode was electrically coated by polyaniline (PANI) and its nanocomposites comprising of TiO_2, Ag, and Zn. The prepared coatings were characterised by FT-IR, SEM, EDS, UV-vis and optical microscopy techniques. Further as a continuation, **Murat Ates *et al.,*** tested the corrosion behaviour of A11050 electrode in absence and presence of PANI, PANI/TiO_2, PANI/Ag and PANI/Zn nanocomposite under 3.5% NaCl medium. Comparing the results obtained from impedance and polarisation methods, it was concluded that PANI/Ag rendered greater metal protection[26].

Madhan Kumar *et al.,* reported the reduced corrosion and bacterial growth on the surface of mild steel by using novel TiO_2-CuO nanocomposite as nanofillers within the epoxy coatings. Phase composition as well as morphology of the prepared composites were characterised by Raman spectra, SEM and EDS analysis. The corrosion inhibition studies carried out in 3.5% NaCl medium using electrochemical measurements projected enhanced performance of TiO_2-CuO nanocomposites than epoxy coatings alone[27].

Bis-[triethoxysilylpropyl] tetrasulfide silane (BTESPT) with SiO_2 or CeO_2 nanoparticles based pretreatment carried out for galvanised steel substrates by **Montemor *et al.,*** was extended to electrochemical impedance technique in order to access the corrosion behaviour. The results obtained concluded that the barrier formation was facilitated by nanoparticles thereby reducing the corrosion process where the CeO_2 nanoparticles were found to be more predominant than SiO_2 nanoparticles[28].

Sam John *et al.,* utilised sol-gel and dip coating process to coat nanochitosan/ZnO nanoparticles on the mild steel surface. The surface film formed were characterised by FT-IR, XRD, SEM, EDS and UV-vis spectroscopy. Based on potentiodynamic polarisation, linear polarisation and impedance spectroscopy studies (EIS) the corrosion behaviour of coated specimens under 0.1 N HCl solution were explored[29].

Moses M. Solomon *et al.*, approached a green method to synthesise gum Arabic-silver nanoparticles (GA-AgNPs) which was characterised by FTIR, UV-vis, EDAX and SEM analysis. Corrosion inhibition rendered by GA-AgNPs for steel specimens in 15% H_2SO_4 and HCl medium was assessed by mass loss, electrochemical and surface morphological studies. Studies made portrayed mixed type of inhibition in 15% H_2SO_4 and anodic nature in 15 % HCl. Both the inhibition was found to obey Langmuir adsorption isotherm. In addition XPS analysis was also carried out to study the mechanistic action of inhibitors[30].

Kanagalasara Vathsala *et al.*, utilised electrodeposition techniques to synthesise Zn and Zn–ZrO_2 composite coatings. Followed by the characterisation of coatings by SEM and XRD, its corrosion resistance ability was examined based on open circuit potential (OCP) and Tafel analysis in 3.5 wt% NaCl solution. The results obtained were in such a way that Zn–ZrO_2 coatings dominated over Zn coating[31].

Polypropylene glycol/silver nanoparticles (PPG/AgNPs) was synthesised by **Moses M. Solomon *et al.*,** as a novel composite which was characterised by TEM analysis to explore its spherical nano form, XRD and EDS results to confirm the dispersion of nano particles. Effect of these synthesised composites in protecting the mild steel specimens under 0.5 M H_2SO_4 were studied using electrochemical and non-electrochemical techniques. At a temperature range of 333 K, 94% of inhibition efficiency was noticed. Mixed type of inhibition was revealed from polarisation studies. Best fit was observed with Temkin isotherm. Further the film formed after immersion was confirmed by SEM, EDS and contact angle measurements[32].

Epoxy (E) nickel oxide (NiO) nanocomposite materials were successfully synthesised by **Madhup *et al.*,** where a high dispersion of nickel oxide nanoparticles was done in epoxy resin (containing diglycidyl ether of bisphenol A (DGEBA)). FT-IR, SEM, XRD and AFM techniques were used to characterise the nanocomposites. To understand the corrosion inhibition performance, salt spray resistance as per ASTM B-117 test method was carried out for nickel oxide epoxy nanocomposite (NiO-ENC) [33].

Radhakrishnan *et al.*, imparted in situ polymerisation method to synthesise coatings from polyaniline–nano-TiO_2 particles. Corrosion resistance for steel plates were studied in presence of polyaniline (10 wt%) with different concentrations of nano-TiO_2 for a duration of 90 hours exposed to hot saline medium. On investigating the results, 100 times better result was observed for polyaniline with 4.18 wt% nano-TiO_2. This pronounced result was favoured due to the formation of barrier, as well as increased surface coverage with hindrance to charge transfer[34].

Nanocomposite coatings comprising of polybenzoxazine (PB-TMOS) and SiO_2 nanoparticles were applied on the mild steel surface and its corrosion inhibition nature was studied under the influence of silica content by means of electrochemical measurements by **Changlu Zhou *et al.,*** FT-IR, SEM and ^{29}Si NMR analysis was used to study the morphology. The covalent bond between polymer (PB-TMOS) and nano particles enhanced the corrosion inhibition due to the resulting interfacial interactions[35].

Jinlong Hu *et al.,* synthesised polymer–clay nanocomposites (PANI/AD-LDH) and its corrosion resistance was measured by open circuit potential, potentiodynamic polarization and electrochemical impedance spectroscopy (EIS) in 3.5% NaCl solution. The obtained results revealed that PANI/AD-LDH offered better corrosion inhibition than PANI and D-LDH[36].

AA-1050 metal substrate was chosen by **Sharifi Golru *et al.,*** to study its metal dissolution phenomena under the influence of Al_2O_3 nanoparticles (1, 2.5 and 3.5 w/w) on epoxy/polyamide coatings. Nano dispersion was confirmed by UV-vis and FE-SEM. Electrochemical impedance spectroscopy studies was made for a duration of 135 days in 3.5% NaCl solution. The added nanoparticles retarded corrosion by reducing water and hydrolytic degradation[37].

Graft polymer Ch-*g*-mPEG (Chitosan (Ch), poly(ethylene glycol)(PEG)) was synthesised and characterised using FT-IR, XRD, ^1H NMR and GPC analysis by **Hassan *et al.,***. Incorporation of silver nano particles within Ch-*g*-mPEG composite was confirmed by HRTEM and EDAX. As an application, the synthesised composites with and without silver nanoparticles were tested for its inhibition mode for carbon steel in 1M aggressive HCl medium. From the results obtained from electrochemical measurements, pronounced inhibition efficiency was offered by Ch-*g*-mPEG self-assembled on silver nanoparticles than Ch-*g*-mPEG only. Both the methods favoured increased inhibition efficiency on increasing the concentration[38].

Moses M. Solomon *et al.,* observed a pronounced increase in inhibition efficiency of St37 steel in 15% H_2SO_4 solution from 45% (in presence of chitosan alone) to 94% (in presence of AgNPs-Chi composite). Resisted corrosion in presence of chitosan and silver nanoparticles (AgNPs-Chi) was studied by electrochemical and non-electrochemical techniques. Best fit was observed with Langmuir adsorption isotherm. Both anodic and cathodic redox reactions were controlled by AgNPs-Chi composites. Surface studies also supported the same[39].

Mohammad Ali Asaad et al., documented the corrosion resistance rendered by *Elaeis guineensis* (EG) and silver nanoparticles (AgNPs) on mild steel in 1 M HCl medium. The structural elucidation of EG/AgNPs was done by TEM, XRD, and EDX analyses. Mild steel

specimens were subjected to weight loss, impedance and polarisation techniques followed by its surface study by FE-SEM, EDX, AFM and XRD. 94.1% of inhibition efficiency was obtained for 10% (v/v) of EG/AgNPs inhibitor[40].

Cerium oxide nanoparticles precipitated from $Ce(NO_3)_3.6H_2O$ in water was used as effective corrosion retarders for mild steel by **Fedel *et al.,***. Particles obtained were of 70 nm in diameter. From the impedance and open circuit potential measurements, contributions made by ceria nanoparticles were highly projected resulting in ennoblement effect[41].

Ghasem Bahlakeh *et al.,* reported the influence of cerium oxide nanoparticles (CeONPs) on metal protecting ability of melamine-cured polyester (MCP) resin. Cathodic delamination test and electrochemical impedance spectroscopy were used to explore coating disbondment and corrosion resistance. Better corrosion resistance was observed due to strong CeONPs/MCP bonds thereby strengthening adhesion[42].

Development of novel class of active inhibitors comprising of CeO_2 nanoparticles and polyaniline was documented by **Sasikumar *et al.,*** The structural confirmation of PANI/CeO_2 nanocomposite (PCN) was made by XRD, IR, XPS, SEM and TEM analysis. The inhibition effect of PCN on mild steel in 0.5 M HCl was studied by electrochemical and gravimetric techniques. Potentiodynamic polarisation suggested mixed type of inhibition whereas impedance measurements revealed the formation of surface barrier supported by morphological analysis by ATR-IR, SEM/EDAX and AFM techniques[43].

Solomon *et al.,* prepared poly(methacrylic acid)/silver nanoparticles (PMAA/AgNPs) composite by in-situ polymerisation method followed by its characterisation by FTIR, TEM, XRD, EDS and UV-vis spectroscopy. Increasing the concentration of PMAA/AgNPs resulted with an increase in inhibition efficiency which revealed the formation of film on the steel surface. Experimental results were best fitted with Temkin adsorption isotherm model. Mixed type of inhibition was suggested from Tafel analysis[44].

In order to rectify the permeability nature of coatings which could not be eliminated, addition of inhibitors in nano forms along with coatings can be adopted. This method was experimented by **Sharmila *et al.,*** who utilised nano cerium oxide as inhibitor under H_2SO_4 and HCl medium for a duration of 24 hours at room temperature by mass loss method. The results favoured better inhibition efficiency in sulphuric acid medium rather than HCl medium[45].

Reviewing of several articles let to know the limited work carried out using biosynthesised nano forms which provided us a preliminary platform to inculcate this method in the present discussion. The above literature clearly shows the impact of nano materials alone or in combination with polymers which is added instantaneously as per the requirements. With

this intention, avocado seeds which has attained considerable attention has been chosen to form a preliminary platform of synthesising transition metal oxides like zinc oxide (ZnO), copper oxide (CuO) and Tin oxide (SnO) targeting towards profitable and eco-friendly environment. This dispersion of biosynthesised nano forms within the polymeric backbone is certainly a new approach which has not been done so far. With a motto of framing a new method, as well as limited work carried out with polyesters made us to synthesise nano metal oxide dispersed polyesters namely polymer nano metal oxide composite (PNMOC) for the first time and to document its enhanced metal protecting ability compared with the parent precursors as discussed in the previous chapter III.

5.2 EXPERIMENTAL METHODS

5.2.1 Chemicals and metal substrate

Zinc acetate dihydrate ($Zn(COOCH_3)_2.2H_2O$), stannous chloride ($SnCl_2$), cupric chloride ($CuCl_2$), ethanol, sodium hydroxide (NaOH) were procured and used as such. Whereas *Persia Americana* seeds were powdered and used. Double distilled water based 0.5 M H_2SO_4 was prepared from analytical grade. As per the ASTM standards the mild steel coupons were machined and used.

5.2.2 Synthesis

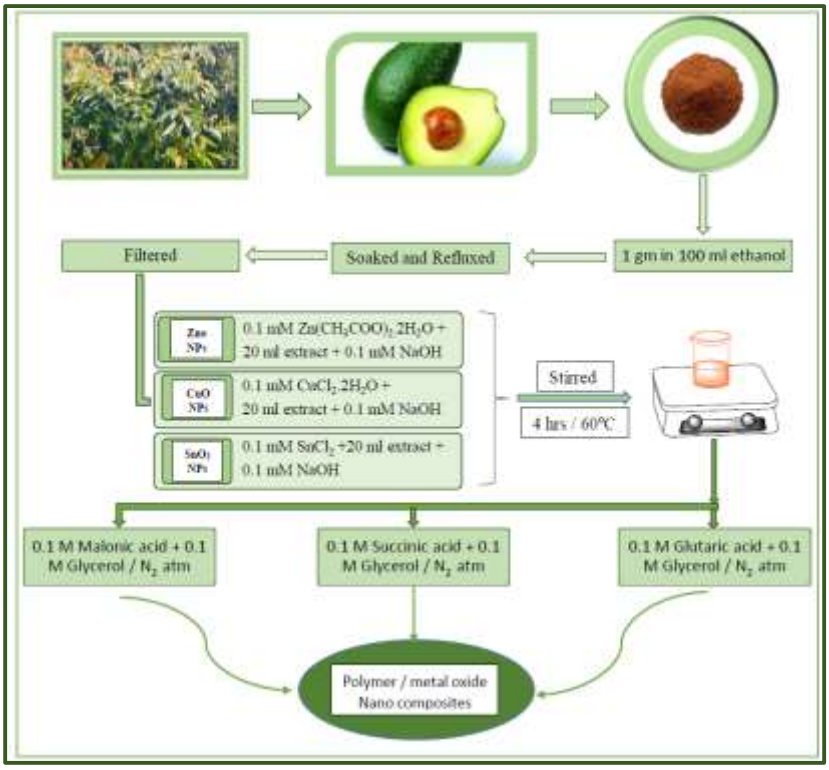

Fig. 1 Schematic illustration of synthesis

Synthesis of polymer-nano metal oxide composites (PNMOC) were done adopting the method as shown in **Fig. 1**

(i) Preparation of extract

Persia Americana generally termed as avocado was collected followed by the separation of seeds. The seeds used as precursors were washed with double distilled water, shade dried and milled into fine powder. With an intention of purifying it further it was given a petroleum ether wash followed by drying and storing for further proceedings.

About 1 gram of powdered seed was soaked in 100 ml ethanol in a beaker, closed and kept aside overnight. The mixture was then refluxed for stipulated time until a dense colour change was observed. It was left undisturbed for few hours. The supernatant liquid was filtered and refrigerated.

(ii) Biosynthesis of polymer-nano metal oxide composites (PNMOC)

To start with nano metal oxides, 0.1 mM proportion of the respective salt was taken along with 20 ml of ethanolic extract accompanied with continuous stirring for 4 hours at 60^{o}C which is a slight modified method from the report of **Ganesh Elango *et al.,***[46] . The resulting mixture was allowed to disperse in the polymerisation reaction occurring between dicarboxylic acids (0.1 M) and glycerol (0.1 M) in nitrogen atmosphere (discussed in chapter II) leading to polymer-nano metal oxide composites (PNMOC).

It is noticeable that the added plant extract has the capability of reducing and stabilising the added salts[47] due to the presence of alkaloids, glycosides, phenols and saponins present in the ethanolic extract as investigated by **Ruth *et al.,***[48].

5.2.3 Characterisation techniques

(i) Fourier Transform Infrared spectroscopy (FT-IR) and X- ray diffraction (XRD) analysis

The polymer-nano metal oxide composites (PNMOC) were characterised using Fourier Transform Infrared spectroscopy (FT-IR) by Schimadzu – FTIR spectrometer in the range of 4000 – 400 cm^{-1} with an additional evidence of X-ray diffraction analysis acquired through Brucker X- ray diffractometer with 2Ɵ ranging from 0 to 80^{o}.

(ii) Scanning electron microscopy (SEM) and Energy dispersive X-ray spectroscopy (EDS)

Energy dispersive X-ray spectral (EDS) analysis of the polymer nano metal oxide composites were analysed attached with ZIESS scanning electron microscopy (SEM) analyser.

(iii) Transmission electron microscopy (TEM) analysis

High resolution Transmission electron microscope (Tecnai, G2 20 Twin) was used to analyse the size and shape of nano particles dispersed within the polymer. A drop of sample loaded on copper grid was allowed to dry followed by recording TEM images.

5.2.4 Evaluation of corrosion inhibition activity

(i) Gravimetric measurements

The extent of support rendered by the polymer-nano metal oxide composites (PNMOC) were evaluated by the mass loss method with a work place set up of 100 ml 0.5 M H_2SO_4 test solution with selected concentrations of PNMOC in which precleaned and weighed metal coupons of appropriate dimensions were freely suspended for 3 hours. The retrieved coupons after the stipulated time were washed, dried and reweighed with micro analytical balance. The efficiency of PNMOC were visually examined by calculating the difference in weight loss (mg) which is an average of duplicate measurement. The thickness of the metal lost in the absence and presence of inhibitor was computed in terms of corrosion rate expressed as below,

$$\text{Corrosion rate (CR)} = \frac{534 \text{ X weight loss (gms)}}{\text{Density X Area (cm}^2\text{) X Time (hrs)}} \quad (1)$$

On the other hand, the inhibition efficiency rendered by the added polymer-nano metal oxide composites were evaluated from the following expression,

$$\text{Inhibition efficiency (\%)} = \frac{CR_o - CR_{inh}}{CR_o} X100 \quad (2)$$

where CR_o and CR_{inh} represents the corrosion rate in the presence and absence of inhibitors.

(ii) Electrochemical measurements

Electrochemical tests were performed with a classical three electrode network where platinum and calomel electrode takes the role of counter and reference electrode whereas mild steel rod shaped with 0.785 cm^2 exposed area serves as working electrode. The function associated with the calomel electrode is to provide large area that could provide the current generated for working electrode. Prior to each measurement mirror finish polish was ensured.

Electrochemical impedance and polarisation studies were recorded when steady state open circuit potential irrespective of time was achieved. To start up with impedance measurements, a frequency range of 10 KHz to 0.01 Hz with an amplitude of 10 mV was applied from which the parameters evaluated were used to calculate the inhibition efficiency as per the below equation,

$$\text{Inhibition efficiency}(\%) = \frac{R_{ct(inh)} - R_{ct(blank)}}{R_{ct(inh)}} X100 \quad (3)$$

Undisturbed electrochemical workstation favoured the potentiodynamic polarisation measurement at a potential of ± 200 mV at a scan rate of 1mV/sec.

$$\text{Inhibition efficiency}(\%) = \frac{I_{corr(blank)} - I_{corr(inh)}}{I_{corr(blank)}} X100 \quad (4)$$

where charge transfer resistance and corrosion current density are indicated by R_{ct} and $I_{corr.}$

Both the techniques utilised computer assisted IVIUM compactstat software to generate Nyquist plot (Impedance measurements) and Tafel plot (Polarisation technique) from which a detailed illustration in prevention of metal dissolution can be obtained.

5.3 RESULTS AND DISCUSSION

5.3.1 Characterisation techniques

(i) Fourier Transform Infrared spectroscopy (FT-IR) and X- ray diffraction (XRD) analysis

FT-IR: The FT-IR spectrum recorded for poly(glycerol malonate) (PGM) as well its dispersion with respective nanoparticles is shown in **Fig. 5.1(a)**. The bands observed for –OH linkages, >C=O group and –C-O-C- linkages at 3361.51cm^{-1}, 1716.25 cm^{-1} and 1240.41 cm^{-1} of the precursor (PGM) has undergone some modifications in intensity and shift when filled with nano metal oxides. The formation of nano metal oxides were confirmed by observing bands around 410 cm^{-1} for ZnO[49]. The stretching modes of Sn-O-Sn was predicted around 650 cm^{-1} [50] and 928 cm^{-1}. CuO stretching vibration near to 600 cm^{-1} [51]confirmed the presence of CuO nano particles. Similar changes were viewed in case of poly(glycerol succinate) (PGS) as well its dispersion with respective nanoparticles as shown in **Fig. 5.1(b)**. The bands observed for –OH linkages, >C=O group and –C-O-C- linkages at 3392.51 cm^{-1}, 1713.24 cm^{-1} and 1163.23 cm^{-1} of the precursor (PGS) has undergone a shift from its original position when filled with nanometal oxides. The formation of nano metal oxides was confirmed by observing bands around 410 cm^{-1} for ZnO in PGS-ZnO NPs. The stretching modes of Sn-O-Sn were predicted

around 680 cm^{-1} and 900 cm^{-1} in PGS-SnO NPs which is slightly deviated from the already stated report. Cu-O stretching vibration appeared around 600 cm^{-1} and 479 cm^{-1} in PGS-CuO NPs owing to the presence of nanofillers. However mild stretching vibration around 535 cm^{-1} would be due to the maximum encapsulation of nano metal oxide by polymer additives. The shifts observed in the nano-dispersed form with respect to the parent precursor (PGS) as well as the deviation from the expected stretching modes, could be due to the possible interaction of nano metal oxides with PGS moieties with minimum structural modification of the poly(glycerol succinate) which is evident from the presence of main bands of PGS in nano dispersed form. **Fig. 5.1(c)** represented FT-IR spectra of poly(glycerol glutarate) (PGG) and its nano dispersed forms confirming the dispersion of nano fillers within polymer matrix. The shifts differing from the parent precursor clearly proved that the nano metal oxides has well bound with polymer moieties.

XRD: Figs. 5.2(a-c) shows the XRD patterns recorded for parent polymer and dispersion forms using Cu as a target material. The amorphous nature of the precursors is noticed from the figures with a hump at $2\Theta = 20^{o}$ [52,53]. Looking into the rest of the patterns well coincided with JCPDS. No of 79.2205, 80.1916, 77.2296 owing to ZnO (hexagonal), CuO (monoclinic) and SnO (orthorhombic) nano metal oxides. **Fig. 5.2(a)** showed the dispersed ZnO nano peaks at 31.86 (100), 36.33 (101) followed by CuO peaks at 36.1 (111) and SnO peaks at 24.34 (111) and 31.14 (020) within the parent (PGM) matrix which coincided well with JCPDS reference patterns. In **Fig. 5.2(b)**, similar dispersion allowed to elicit the peaks at 31.44 (100), 36.93 (101) and 47.80 (102) corresponding to PGS-ZnO NPs with CuO dispersion at 35.21 (111) and 38.73 (111) and SnO at 25.9 (111) within the backbone of PGS. **Fig. 5.2(c)** comprised the patterns of PGG-metal oxide NPs with characteristic peaks at 36.45 (101) for ZnO and 32.45 (110), 46.71 (112) for CuO and SnO at 30.9 (020), 46.4 (024), 53.2 (025). All the three diffracted patterns showed the amorphous back bone of polymer along characteristic nano metal oxide peaks.

The particle size distribution was calculated using Scherer's equation as given below

$$D=K\lambda / \beta\cos\Theta \quad (5)$$

where D, K and β refers to particle size, Scherer constant (0.94) and Full width half maxima. Θ is the diffraction angle. From the above equation SnO, ZnO and CuO nano particles were found to be in an average of 68 nm, 42 nm and 17 nm for PGM –nano metal oxide composites, 25.31 nm, 23.52 nm and 12.92 nm for PGS –nano metal oxide composites and 22.21 nm,

11.08 nm and 10.11 nm for PGG –nano metal oxide composites. The mild peaks observed might be due to the maximum encapsulation of nano fillers by the polymers[53] which is again ensured by the disturbance occurring at 20^{o} when the parent polymer gets interacted with M-O nanoparticles[54].

(ii) Scanning electron microscopy (SEM) and Energy dispersive X-ray spectroscopy (EDS)

Surface topography of polymers and polymer –nano metal oxide composite (PNMOC) were recorded using sputter coating technique on gold sheets to analyse the dispersion of nanomaterials. **Fig. 5.3(a)** represented a smooth polished image of a neat polyester poly(glycerol succinate) (PGS)[55]. Observation of **Fig. 5.3(b-d)** clearly pictured the dispersion of nano metal oxides within the polymer matrix as documented by **Obaid Ur Rahman *et al.*,**[56]. From the figures it can be understood that minimum agglomeration favoured good dispersion of nano particles which could be reasoned for better results.

The corresponding EDS images shown in **Fig. 5.3(a)** differed from the rest of the three nano blended images clearly confirming the dispersion of nano metal oxides as evident from its peak. In addition, the atomic % of elements depicted in **Table 5.1** also supported the same. The atomic % of carbon and oxygen was found to be around 33% and 66% in all the cases where the minimum intense peaks of 0.14% of Sn (**Fig. 5.3(b))**, 0.22% of Zinc in **Fig. 5.3(c)** and 0.8% of Cu in **Fig. 5.3(d)** endeavoured its presence in polymer–nano metal oxide composite (PNMOC).

(iii) Transmission electron microscopy (TEM) analysis

Fig. 5.4a-d) shows the TEM images of polymer, poly(glycerol succinate) (PGS) and it corresponding nano dispersed forms. Observation of these images shows the nano metal oxide dispersed are of various size and shape which could be due to the usage of bio-reducing agent as well as due to the formation of nano particles at different time intervals. Poly dispersion of nano metal oxides revealed the encapsulation of nano metal oxides within the polymer matrix with minimum agglomeration.

5.3.2 Evaluation of corrosion inhibition activity

(i) Gravimetric measurements

As discussed in chapter III, the inhibition efficiency (%) at an optimised concentration of 1000 ppm of PGM, PGS and PGG polyesters was 56.64 %, 57.35% and 59.61%. As a motto of increasing its potential to a desired level, this present mass loss study has been carried out with similar concentrations (10, 50, 100, 500, 1000 ppm) of PNMOC. The data shown in the **Table 5.2** clearly predicts the influence of nano metal oxides in increasing the efficiency up to 97.82% (PGG-CuO NPs) from 59.61% (PGG) at 1000 ppm concentration which is a drastic change compared to parent precursor polymer PGG. Examination at 10 ppm concentration of nano dispersed forms exhibited lower inhibition efficiency which might be due to the presence of insufficient amount of nano metal oxides. Successive increase in concentration clearly demonstrated that the polymer was well complexed with nano metal oxides facilitating stronger adsorption and higher surface coverage. It is noticed that the greater proportion of nano metal oxide dispersed at higher concentration has the capability of decreasing the hydrophilicity[57] on the metal surface where one can expect the enhanced adsorption due to its high specific surface area[58] offering minimised metal dissolution. Keen observation of the data represented a combined effect of methylene moieties exhibiting +I effect along with nano metal oxides favouring adsorption of PNMOC on the metal substrate. However it has been referred by the corrosion scientists that, presence of methylene groups in polymers could endeavour partial solubility in aqueous medium thereby rendering minimum inhibition efficiency[59,60]. But the added nano metal oxides could overcome this limitation by decreasing the hydrophilicity on the mild steel surface as well as promoting the adsorption of polymeric inhibitors on the mild steel surface. As per the report stated by **Khanna *et al.*,**[61], polymer nano metal oxide composites have a specificity of forming metal chelates which gets adsorbed on the metal surface forming a barrier.

(ii) Electrochemical measurements

(a) Electrochemical impedance spectroscopy (EIS)

The Nyquist plots recorded for 0.5 M H_2SO_4 test medium in the absence and presence of inhibitor with response to frequency change is shown in **Fig. 5.5** and **Figs. 5.6(a-i)**. Observing these plots showed successive increase in the diameter of the semicircles on addition of selected concentrations (10, 100, 1000 ppm) of PNMOC which is obviously recognised with opposite effect between charge transfer resistance (R_{ct}) and double layer capacitance (C_{dl}) as seen from **Table 5.3**. The Nyquist plots displayed is accompanied with an imaginary (–Zimg)

and real (Zreal) parts that can relate frequency signals, polarisation and solution resistance along with double layer capacitance[62].

Observation of the Nyquist plots of parent precursors shown in **Fig. 5.5**, revealed a single semicircle implying that the mechanism of corrosion is controlled by charge transfer process[63,64]. But the increased diameter of the loop in presence of nano metal oxides displayed in **Figs. 5.6(a-i)** insisted that the mechanism remains the same where the charge transfer took place in a slower rate. Increase in the size of the loop shows the intrusion of nano metal oxides within the polymer matrix thereby increasing the charge transfer resistance (R_{ct}).The increased R_{ct} values favoured increase in surface barrier[65] with no modifications in the shape of semicircle implying that the corrosion mechanism remains the same[66]. Impurities, grain boundaries, inhomogeneity and roughness are the factors where one or all brings deviation from the perfect semicircles[67]. Alternatively the double layer capacitance (C_{dl}) decreases on increase in concentration of PNMOC which is still lower compared to parent precursors (PGM, PGS and PGG) due to either gradual displacement of water molecules by the adsorption of inhibitors on metal surface[68] or might be due to hydrophobic nature[56] generated by the nano fillers dispersed. This decrease in C_{dl} is accompanied with increase in thickness of protective layer which follows the trend of Helmholtz model given by

$$C_{dl} = \frac{\Sigma\Sigma_o A}{d}$$

where d, Σ, Σ_o and A represents thickness of double layer, dielectric constant of medium, vaccum permittivity and electrode surface area.

One of the possible method of deducting the electrochemical parameters is by fitting the experimental data with Randle's equivalent circuit as shown in **Fig. 2** where a parallel combination of R_{ct} and constant phase element (CPE) is in series with solution resistance (R_s) as observed.

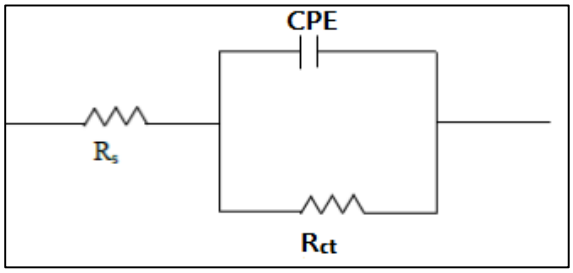

Fig. 2 Randle's equivalent circuit model

Instead of the ideal capacitor, CPE is used in order to get accurate fit as well as to account for the deviations from ideal dielectric nature arising due to the depressed nature of electrode surface. Impedance function of CPE could be represented as per the below equation[67]

$$Zcpe = A^{-1}(j\omega)^{-n}$$

where A refers to CPE constant, n indicates surface irregularity where the angular frequency is denoted by the term ω.

Compared to chapter III, greater inhibitive nature is undoubtedly accredited due to the presence of nano metal oxides behaving as nano fillers in interstitial space of parent polymer (PGM, PGS and PGG) thereby inducing good locking effect[56]. The enhanced inhibition efficiency of PGG-CuO NPs (87.08%), PGG-ZnO NPs (81.50%) and PGG-SnO NPs (70.63%) at 1000 ppm from its precursor PGG (51.53%) is because of nano dispersion owing to fast adsorption kinetics and greater number of particles to be adsorbed[66] creating a passivation capability of PNMOC[69] depending on its concentration which could be similarly reasoned in the remaining PGS and PGM dispersions.

(b) Potentiodynamic polarisation measurement

The potentiodynamic polarisation parameters obtained by sweeping the potential between ± 200 mV at a scan rate of 1mV/sec is displayed in **Table 5.4**. The Tafel plots corresponding to the selected concentration of inhibitors (10, 100, 1000 ppm) PGM, PGS and PGG are displayed in **Fig. 5.7** followed by its nano dispersed Tafel plots in the **Figs. 5.8(a-i)**. The decrease in I_{corr} values from 896.52 µA/cm^2 (uninhibited) shows that the working electrode has undergone polarisation. In general corrosion reaction is associated with either passage of metal ions into the solution (anode) or discharge of hydrogen ions (cathode)[70]. The insertion of inhibitors play a dual role of affecting either cathodic or anodic or both. Examination of the plots, showed the shift in E_{corr} values towards negative direction suggesting the inhibitors to be of cathodic nature. The maximum difference between the E_{corr} values of blank with inhibited ones was about 36.4mV, whereas ± 85mV/ SCE is the threshold factor to decide anodic or cathodic nature. But the present study suggests mixed type of inhibition but predominantly cathodic nature. The decrease in corrosion current density (I_{corr}) proved the protection mode rendered by PNMOC thereby forming a barrier on the metal surface[71]. Also it is clear from the data that the dispersed nano fillers block the active sites responsible for metal dissolution[68] through geometric blocking effect as well as enhancing corrosion protection properties like

water repellency, migration of corrosive ions due to the cross linking nature[72] and generating a passive layer on the metal surface[73].

Generally a corrosion reaction takes the below representation comprising of both cathodic and anodic reactions,

$$4Fe + 3O_2 + 2H_2O \longrightarrow 2Fe_2O_3.\ H_2O$$

However the presence of nanoparticles reduces the water and oxygen permeability towards the metal surface thereby generating greater corrosion mitigation[74]. This statement is additionally evident from the drastic change observed in I_{corr} values from 896.52 µA/cm^2 to 142.91 µA/cm^2 in case of 1000 ppm of CuO dispersed poly(glycerol glutarate) (PGG) polyester which in the presence of parent precursor (PGG) is around 475.63 µA/cm^2. ZnO and SnO dispersed forms of PGG have significantly higher I_{corr} values of 293.79 µA/cm^2 and 234.08 µA/cm^2 that can obviously stimulate metal dissolution at a higher rate compared with CuO dispersion. PGM, PGS and its nano dispersed forms also experienced lower corrosion current density (I_{corr}) on increasing the concentration of inhibitors. However the slight variation observed in inhibition efficiency of all the three investigated systems (PGM, PGS and PGG) in presence of nano fillers evidenced from gravimetric and electrochemical measurements could be attributed due to the fact that, former case is evaluation of average corrosion rate whereas the later depicts instant corrosion rate[75].

5.3.3 Mechanism

A detailed mechanism in protecting the metal substrates is proposed in **Fig. 5.9** Generally the addition of nano fillers enhances the reduced metal dissolution by any of the following ways[56].

(i) Forming a strong barrier thereby preventing the penetration of corrosive ions at metal – electrolyte interface.
(ii) Electrostatic interaction between charged metal substrate and PNMOC
(iii) Favouring good adhesion and locking effect

However the pronounced inhibition efficiency depends on many factors such as active sites, molecular size and mode of interaction. In the present case, the added polymers get adsorbed on the metal surface through its electronegative oxygen atoms. But this adsorption is limited to the existing form of polymers where usually the polymers is expected to be in the form of polycations in acidic medium[76,77]. When the metals are immersed in

0.5 M H_2SO_4 test medium, an array of SO_4^{2-} ions are generated creating excess negative charge[78] on the metal surface which is then electrostatically attracted by the positively charged PNMOC forming an adherent barrier[79]. The low inhibition efficiency observed for parental precursors (PGM, PGS and PGG) would be due to the incapability of anions of aggressive medium which is a main key factor in generating the excess negative charge (SO_4^{2-}) that can facilitate the attraction of polycations. From the measurements carried out it is undoubted that the addition of nano materials has increased the inhibition efficiency compared to the parent polymer due to its hydrophobic surface coverage ability.

The nano fillers with polymer matrix smartly works by reducing the generation of corrosive ions as well as by departing specific areas from the aggressive environment through an enhanced protective layer[80]. It is generally assumed that the nano metal oxides would have been encapsulated by the polymer matrix followed by the successive adsorption on the metal substrate by –O-M-O- bonds increasing its surface coverage as suggested by **Balaji *et al.*,**[81]. PNMOC gets adsorbed on the metal surface, where nano fillers within the composite reacts with the metal surface and reduced the repulsive force exerted by the metal surface on the adsorbed layer ie., favours good adsorption rather than desorption.

5.4 CONCLUSIONS

(i) Biosynthesised nano metal oxide dispersed polymer matrix ie., polymer-nano metal oxide composites (PNMOC) were synthesised.

(ii) The synthesised PNMOC were characterised by FT-IR, XRD, SEM-EDS and TEM analysis to confirm the dispersion of nano metal oxides.

(iii) Addition of PNMOC at various concentrations (10, 50, 100, 500, 1000 ppm) were favoured enhanced inhibition efficiency in 0.5 M H_2SO_4 test medium.

(iv) On increasing the concentration, enhanced ability of protecting the metal coupons up to 97 % was achieved from non-electrochemical method.

(v) Increased R_{ct} and decreased I_{corr} values from electrochemical measurements favoured increased inhibition efficiency.

(vi) A comparison of inhibition efficiency rendered by parent precursors (PGM, PGS and PGG) with that of nano dispersed forms were made.

(vii) Combined synergistic effect observed between the encapsulated nano metal oxides and polyesters contributed to the enhanced protection of mild steel surface in acid medium.

(viii) Average particle size evaluated from XRD patterns revealed the particle size in the order of SnO > ZnO > CuO in all the polymer-nano metal oxide composites owing to a confirmation that CuO being smaller in size rendered maximum surface coverage.

5.5 REFERENCES

1. M. R. Noor El-Din, R.K. Farag, O.E. Elazbawy, Int. J. Electrochem. Sci., **11** (2016) 815-835.
2. X. Su, C. Lai, L. Peng, H. Zhu, L. Zhou, L. Zhang, X. Liu, W. Zhang, Int. J. Electrochem. Sci., **11** (2016) 4828-4839.
3. C.B. Verma, M.A. Quraishi, E.E. Ebenso, Int. J. Electrochem. Sci., **9** (2014) 5507-5519.
4. M.R. Vinutha, T.V. Venkatesha, Portugal. Electrochim. Acta., **34(3)** (2016) 157-184.
5. G.Madhusudhana, R. Jaya Santhi, Int. J. Sci. Res., **4(1)** (2015) 1645-1650.
6. F.M. Mahgoub, S. M. Al-Rashdi, *Open J* Phys *Chem.*, **6** (2016) 54-66.
7. J.A. Nasser, M.A. Sathiq, Arabian J. Chem., **9** (2016) S691-S698.
8. Y. Qiang, L. Guo, S. Zhang, W. Li, S. Yu, J. Tan, Sci. rep., **6** (2016) 1-14.
9. K.R. Ansari, S. Ramkumar, D. Nalini, M.A. Quraishi, Cogent. Chem., **2** (2016) 1-15.
10. R.T. Loto, O. Tobilola, J. *King. Saud* Univ Sci., **https://doi.org/ 10.1016/j.jksues. 2016. 10.001** (2016) 1-7.
11. P.A. Lozada , O.O. Xomet, D.G. Lucero, N.V. Likhanova, M.A. Domínguez-Aguilar, I.V. Lijanova ,E.A. Estrada, Mater., **7** (2014) 5711-5734.
12. V. Dharmalingam, P.A. Sahayaraj, A.J. Amalraj, A.A. Prema, J. Adv. Electrochem., **2(1)** (2016) 37-41.
13. R. Karthikaiselvi, S. Subhashini, JAAUBAS., **16** (2014) 74-82.
14. V.K. Thakur, M.K. Thakur, Eco-friendly Polymer Nanocomposites Processing and Properties, Adv. Str. Mater., springer India, (2015) First edition.
15. A. Bhattacharjee, M. Ahmaruzzaman, RSC Adv., **47** (2016) 1-38.
16. E.F.I. Gouegni, Abubakar, Nigerian Food Journal., **31(1)** (2013) 64-69.
17. A.F. Vinha, J. Moreira, S.V. P. Barreira, J. Agric. Sci., **5(12)** (2013) 100-109.
18. D. Dabas, R.M. Shegog, G.R. Ziegler, J.D. Lambert, Curr. Pharm. Des., **19** (2013) 6133-6140.
19. U. Eduok , E. Jossou, J. Szpunar, J. Mol. Liq., **241** (2017) 684-693.
20. R. Alam, M. Mobin, J. Aslam, Surf. Coat. Technol., **307** (2016) 382-391.
21. S.K. Dhoke, A.S. Khanna, Corros. Sci., **51** (2009) 6-20.
22. A.A. Javidparvar, B. Ramezanzadehb, E. Ghasemi, J. Taiwan Inst. Chem Eng., **61** (2016) 356-366.
23. I.A.W. Ma Ammar Sh, K. Ramesh, B. Vengadaesvaran, S. Ramesh, A.K. Arof, Prog. Org. Coat., **113** (2017) 74-81.

24. G. Ebrahimi, F. Rezaei, J. Neshati, J. Taiwan. Inst. Chem. Eng., **70** (2017) 427-436.
25. A.M. Atta, O.E. El-Azabawy, H.S. Ismail, Corros. Sci., **53(5)** (2011) 1680-1689.
26. M. Ates, E. Topkaya, Prog. Org. Coat., **82** (2015) 33-40.
27. M. Kumar, A. Khan, R. Suleiman, M. Qamar, S. Saravanan, H. Dafalla, Prog. Org. Coat., **114** (2018) 9-18.
28. M.F. Montemor, M.G.S. Ferreira, Electrochim. Acta., **52(24)** (2007) 6976-6987.
29. S. John, A. Joseph, A.J. Jose, B. Narayana, Prog. Org. Coat., **84** (2015) 28-34.
30. M.M. Solomon, H. Gerengi, S.A. Umoren, N.B. Essien, U.B. Essien, E. Kaya, Carbohydr. Polym., **181** (2018) 43-55.
31. K. Vathsala, T.V. Venkatesha, Appl. Surf. Sci., **257** (2011) 8929-8936.
32. M.M. Solomon, S.A. Umoren, J. Colloid Interface Sci., **462** (2016) 29-41.
33. M.K. Madhup, N.K. Shah, P.M. Wadhwani, Prog. Org. Coat., **80** (2015) 1-10.
34. S. Radhakrishnan, C.R. Siju, D. Mahanta, S. Patil, G. Madras, Electrochim. Acta., **54(4)** (2009) 1249-1254.
35. C. Zhou, X. Lu, Z. Xin, J. Liu, Y. Zhang, Corros. Sci., **80** (2014) 269-275.
36. J. Hu, M. Gan, L. Ma, Z. Li, J. Yan, J. Zhang, Surf. Coat. Technol., **240** (2014) 55-62.
37. S.S. Golru, M.M. Attar, B. Ramezanzadeh, Prog. Org. Coat., **77(9)** (2014) 1391-1399.
38. H.H.H. Hefni, E.M. Azzam, E.A. Badr, M. Hussein, S.M. Tawfik, Int. J. Biol. Macromol., **83** (2016) 297-305.
39. M.M. Solomon, H. Gerengi, T. Kaya, S.A. Umoren, Int. J. Biol. Macromol., **104** (2017) 638-649.
40. M.A. Asaad, N.N. Sarbini, A. Sulaiman, M. Ismail, G.F. Huseien, Z.A. Majid, P.B. Raja, J. Ind. Eng. Chem., **https://doi.org/10.1016/j.jiec.2018.02.010** (2018) 1-33.
41. M. Fedel, A. Ahniyaz, L.G. Ecco, F. Deflorian, Electrochim. Acta., **131** (2014) 71-78.
42. G. Bahlakeh, B. Ramezanzadeh, M. Ramezanzadeh, Corros. Sci., **118** (2017) 69-83.
43. Y.Sasikumar, A. Madhan Kumar, Z.M. Gasem, E.E. Ebenso, Appl. Surf. Sci., **330** (2015) 207-215.
44. M.M. Solomon, S.A. Umoren, E.J. Abai, J. Mol. Liq., **212** (2015) 340-351.
45. R. Sharmila, N. Selvakumar, K. Jeyasubramanian, Mater. Lett., **91** (2013) 78-80.
46. G. Elango, S.M. Kumaran, S.S. Kumar, S. Muthuraja, S.M. Roopan, Spectrochim. Acta A., **145(5)** (2015) 175-180.
47. A.K. Mittal, Y. Chisti, U.C. Banerjee, Biotechnol. Adv., **31** (2013) 346-356.
48. R.E. Kristanty, J. Suriawati, J. Sulistiyo, Int. Res. J. pharm., **5(7)** (2014) 557-559.

49. T. V. Surendra, S.M. Roopan, N.A.A. Dhabi, M.V. Arasu, G. Sarkar, K. Suthindhiran, *Nanoscale* Res Lett., **11(546)** (2016) 1-10.
50. S. Blessi, M.M.L. Sonia, S. Vijayalakshmi, S. Pauline, Int. *J. Chemtech.* Res., **6(3)** (2014) 2153-2155.
51. A. Rahman, A. Ismail, D. Jumbianti, S. Magdalena, H. Sudrajat, Indo. J. Chem., **9(3)** (2009) 355-360.
52. H.K. Inamdar, R.B. Basavaraj, H. Nagabhushana, M. Devendrappa, Mater *Today.* Proc., **3** (2016) 3850-3854.
53. D.P. Valença, K.G. Bezerra Alves, C. Pinto de Melo, N. Bouchonneau, Mater. Res., **18(Suppl 2)** (2015) 273-278.
54. S. Sathiyanarayanan, S. Syed Azim, G. Venkatachari, Synth. Met., **157** (2007) 205-213.
55. K. Trinath, G. Ramanjaneyulu, *Indian* J. Sci. Technol., **9(S1)** (2016) 1-5.
56. O.U. Rahman, S. Ahmad, RSC Adv., **6** (2016) 10584-10596.
57. S.A. Umoren, A. Madhankumar, J. Mol. Liq., **224** (2016) 72-82.
58. O.D. Lewisa, G.W. Critchlowa, G.D. Wilcoxa, A.D. Zeeuwb, J. Sander, Prog. Org. Coat., **73** (2012) 88-94.
59. D. Thirumoolan, V.A. Katkarb, G. Gunasekaranb, T. Kanaib, K.A. Basha, Prog. Org. Coat., **77** (2014) 1253-1263.
60. S.A. Umoren, M.M. Solomon, Open Mater. Sci. J., **8** (2014) 39-54.
61. P.K. Khanna, N. Singh, S. Charan, V.V.V.S. Subbarao, R. Gokhale, U.P. Mulik, Mater. Chem. Phys., **93** (2005) 117-121.
62. G. Xia, X. Jiang, L. Zhou, Y. Liao, M.duan, H. Wang, Q. Pu, J. Zhou, Corros. Sci., **94** (2015) 224-236.
63. Z. Zhang, N. Tian, L.Zhang, L. Wu, Corros. Sci., **98** (2015) 438-449.
64. M.P. Pardave, M.R. Romo, H.H. Hernandez, M. A.A. Quijano, N.V. Likhanova, J. Uruchurtu, J. M. Juárez-García, Corros. Sci., **54** (2012) 231-243.
65. G.N. Devi, J. Saranya, N. Manjubaashini, T.D. Thangadurai, S.M. Roopan, S. Chitra, Prog. Org. Coat., **109** (2017) 117-125.
66. G.A. El-Mahdy, A.M. Atta, H.A. Al-Lohedan, Molecules., **19** (2014) 1713-1731.
67. S. John, A. Joseph, A.J. Jose, B. Narayana, Prog. Org. Coat., **84** (2015) 28-34.
68. A.M. Atta, G.A. El-Mahdy, H.A. Al-Lohedan, S.A. Al-Hussain, Int. J. Mol. Sci., **15** (2014) 6974-6989.
69. C. Hu, Y. Qing, Y. Li, N. Zhang, J Alloys. Compd., **717(15)** (2017) 98-107.

70. M. Atta, G. A. El-Mahdy, H. A. Al-Lohedan, S. A. Al Hussain, Dig J Nanomater Biostruct., **9(2)** (2014) 627-639.
71. F. Alvi, N. Aslam, S.F. Shaukat, Am. J. Appl. Chem., **3(2)** (2015) 57-64.
72. M.R. Shaik , M. Alam, N.M. Alandis, J. Polym. Eng., **35(9)** (2015) 1-12.
73. A. Ganash, J. Nanomater., **2014** (2014) 1-8.
74. M.A. Deyab, S.T. Keera, Mater. Chem. Phys., **146(3)** (2014) 406-411.
75. Z. Tao, W. He, S. Wang, S. Zhang, G. Zhou, Corros. Sci., **60** (2012) 205-213.
76. H.H.H. Hefni, E. M. Azzam, E. A. Badr, M. Hussein, S. M. Tawfik, Int. J. Biol. Macromol., **83** (2016) 297-305.
77. S. A. Umoren, M.J. Banera, T. Alonso-Garcia, C.A. Gervasi, M.V. Mirifico, Cellulose., **20** (2013) 2029-2545.
78. A. Farag, M.A. Hegazy, Corros. Sci., **74** (2013) 168-177.
79. R. Geethanjali, S. Subhashini, Chem Sci Trans., **2(4)** (2013) 1148-1159.
80. S. Ammar, K. Ramesh, B. Vengadaesvaran, S. Ramesh, A.K. Arof, Electrochim. Acta., **220** (2016) 417-426.
81. J. Balaji, M.G. Sethuraman, Prog. Org. Coat., **99** (2016) 463-473.

Table 5.1 Elemental composition from Energy dispersive X-ray spectroscopy (EDS)

Element (%)	PGS	PGS – SnO NPs	PGS – ZnO NPs	PGS – CuO NPs
C	33.31	33.43	33.18	33.56
O	66.66	66.38	66.58	65.51
Zn	-	-	0.22	-
Cu	-	-	-	0.80
Sn	-	0.14	-	-
Au	0.03	0.05	0.02	0.13

Table 5.2 Mass loss datas for various concentrations of polymer- nano metal oxide composites (PNMOC) in 0.5 M H_2SO_4

Name of the Inhibitor	Concentration (ppm)									
	10		50		100		500		1000	
	IE (%)	CR ($gcm^{-2}hr^{-1}$)	IE (%)	CR ($gcm^{-2}hr^{-1}$)	IE (%)	CR ($gcm^{-2}hr^{-1}$)	IE (%)	CR ($gcm^{-2}hr^{-1}$)	IE (%)	CR ($gcm^{-2}hr^{-1}$)
PGM	41.07	11.77	44.21	11.14	44.85	11.01	47.89	10.41	56.64	8.66
PGM-SnO NPs	48.61	10.26	53.08	9.37	55.19	8.95	64.6	7.07	73.43	5.31
PGM-ZnO NPs	71.52	5.69	74.71	5.05	80.35	3.92	82.77	3.44	83.98	3.20
PGM-CuO NPs	82.98	3.40	84.32	3.13	88.36	2.32	95.13	0.97	97.3	0.54
PGS	43.81	11.22	44.98	10.99	45.07	10.97	54.21	9.14	57.35	8.52
PGS-SnO NPs	49.45	10.09	58.33	8.32	66.68	6.65	69.64	6.06	80.17	3.96
PGS-ZnO NPs	75.68	4.86	78.33	4.33	84.25	3.15	85.39	2.92	87.96	2.40
PGS-CuO NPs	83.58	3.28	89.65	2.07	91.34	1.73	94.29	1.14	97.23	0.55
PGG	44.48	11.09	45.72	10.84	46	10.78	56.02	8.78	59.61	8.07
PGG-SnO NPs	52.08	9.57	60.05	7.98	67.78	6.43	72.24	5.54	88.64	2.27
PGG-ZnO NPs	63.21	7.35	66.84	6.62	69.24	6.14	71.68	5.66	74.93	5.01
PGG-CuO NPs	86.02	2.79	91.15	1.77	94.48	1.10	95.3	0.94	97.82	0.44

Table 5.3 AC-impedance parameters for corrosion of mild steel with selected concentrations of polymer- nano metal oxide composites (PNMOC) in 0.5 M H_2SO_4

Name of the inhibitor	Conc. (ppm)	R_{ct} (ohm cm^2)	Cdl ($\mu F/cm^2$)	Inhibition efficiency (%)
Blank	-	15.8	21.5	-
PGM	10	18.2	15.7	13.19
	100	24.3	14.1	34.98
	1000	26.4	12.9	40.15
PGM-SnO NPs	10	28.14	13.2	43.85
	100	32.54	12.5	51.44
	1000	48.95	11.3	67.72
PGM-ZnO NPs	10	47.31	11.9	66.60
	100	60.11	11.1	73.71
	1000	81.03	10.5	80.50
PGM-CuO NPs	10	53.61	10.7	70.52
	100	68.84	9.5	77.05
	1000	108.17	8.3	85.39
PGS	10	20.1	13.7	21.39
	100	27.2	13.5	41.91
	1000	28.9	12.1	45.33
PGS-SnO NPs	10	26.50	13	40.38
	100	39.21	11.8	59.69
	1000	42.24	11	62.59
PGS-ZnO NPs	10	49.84	11.4	68.27
	100	62.5	10.3	74.72
	1000	98.31	8.7	83.93
PGS-CuO NPs	10	48.23	10.4	67.24
	100	95.81	9.1	83.51
	1000	126.04	8.3	87.46
PGG	10	24.3	12.6	34.98
	100	28.4	12.2	44.37
	1000	32.6	11.6	51.53

PGG-SnO NPs	10	35.08	11.9	54.96
	100	41.51	10.1	61.94
	1000	53.8	8.3	70.63
PGG-ZnO NPs	10	31.23	9.7	49.41
	100	41.01	8.1	61.47
	1000	85.42	7.8	81.50
PGG-CuO NPs	10	86.43	9.3	81.71
	100	104.63	7.7	84.89
	1000	122.27	7.1	87.08

Table 5.4 Potentiodynamic polarisation parameters for corrosion of mild steel with selected concentrations of polymer- nano metal oxide composites (PNMOC) in 0.5 M H_2SO_4

Name of the inhibitor	Conc. (ppm)	Tafel slopes (mV/dec)		-Ecorr (mV) vs SCE	I_{corr} ($\mu A/cm^2$)	IE (%)
		b_a	b_c			
Blank	-	63	153	476.9	896.52	-
PGM	10	68	161	479.8	604.43	32.58
	100	69	119	514.5	540.27	39.74
	1000	67	117	528.1	498.23	44.43
PGM-SnO NPs	10	77	143	510.8	517.20	42.31
	100	73	127	492.2	488.96	45.46
	1000	68	136	483.2	401.37	55.23
PGM-ZnO NPs	10	76	129	513.3	344.89	61.53
	100	75	137	500.4	283.12	68.42
	1000	76	145	488.2	214.18	76.11
PGM-CuO NPs	10	64	151	497.2	324.09	63.85
	100	61	143	491	242.87	72.91
	1000	67	142	492.5	186.12	79.24
PGS	10	60	112	512	530.23	40.86
	100	61	114	508.4	525.27	41.41
	1000	62	113	518.1	489.56	45.39
PGS-SnO NPs	10	60	156	503.8	527.96	41.11
	100	64	142	496.2	414.91	53.72
	1000	64	153	500.3	370.80	58.64
PGS-ZnO NPs	10	56	152	499	306.52	65.81
	100	69	139	492.5	251.47	71.95
	1000	67	144	492.4	182.71	79.62
PGS-CuO NPs	10	61	154	502.6	312.89	65.10
	100	64	149	495.2	203.69	77.28
	1000	63	147	488.1	162	81.93

PGG	10	80	188	515.2	525.36	41.40
	100	72	123	470.3	511.58	42.94
	1000	66	115	524	475.63	46.95
PGG-SnO NPs	10	57	151	494.4	512.36	42.85
	100	62	141	488.3	39.81	56.52
	1000	63	132	486.5	234.08	73.89
PGG-ZnO NPs	10	50	156	494.3	436.43	51.32
	100	53	143	491.9	383.98	57.17
	1000	57	133	488.3	293.79	67.24
PGG-CuO NPs	10	61	154	492.5	234.44	73.85
	100	64	149	481.8	185.67	79.29
	1000	67	144	483.6	142.91	84.06

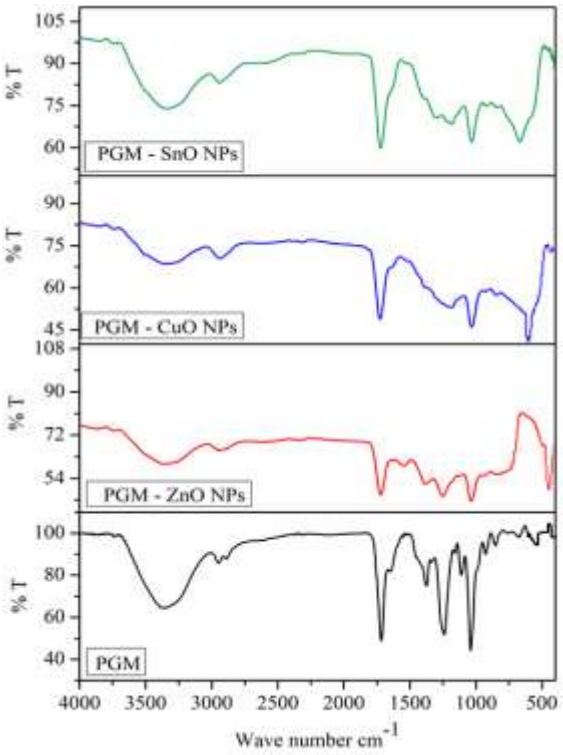

Fig. 5.1(a) FT-IR spectra of PGM-nano metal oxide composites

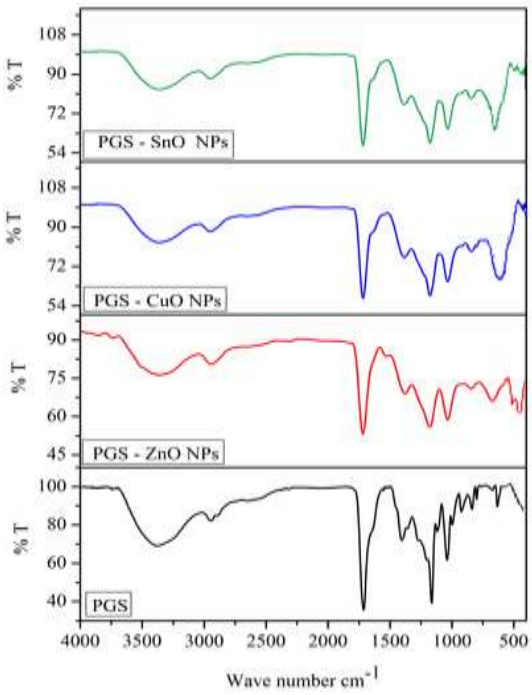

Fig. 5.1(b) FT-IR spectra of PGS-nano metal oxide composites

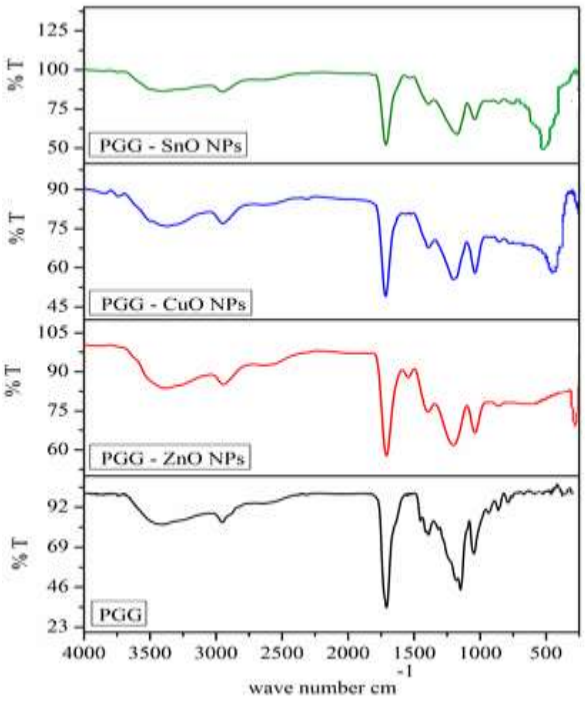

Fig. 5.1(c) FT-IR spectra of PGG-nano metal oxide composites

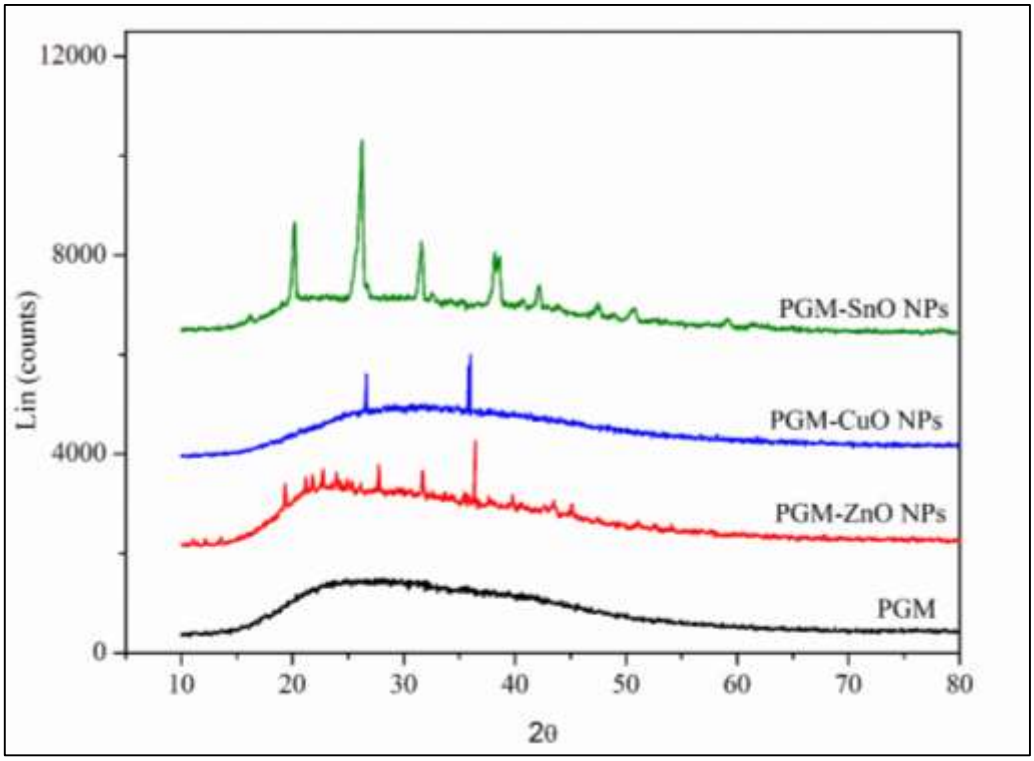

Fig. 5.2(a) XRD pattern of PGM- nano metal oxide composites

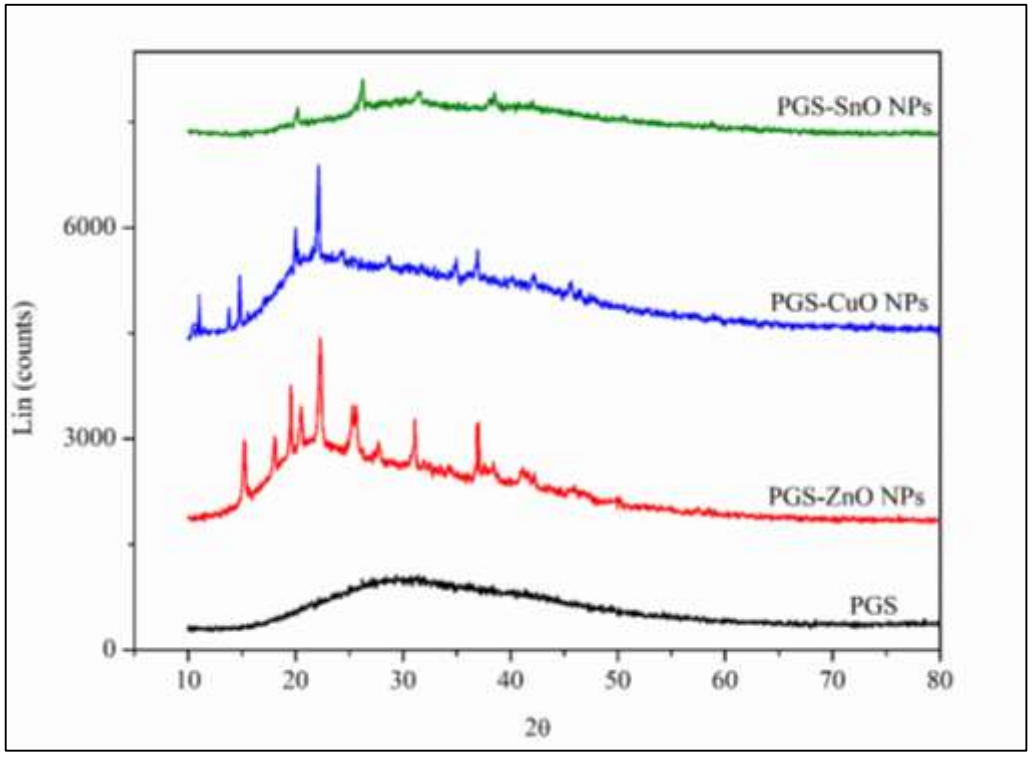

Fig. 5.2(b) XRD pattern of PGS- nano metal oxide composites

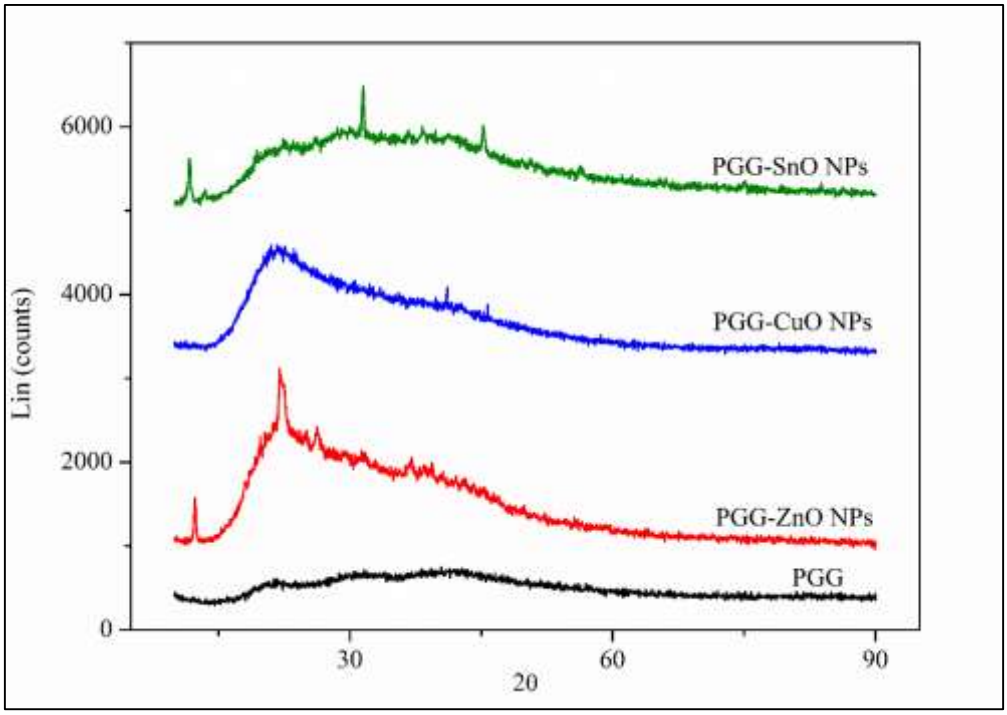

Fig. 5.2(c) XRD pattern of PGG- nano metal oxide composites

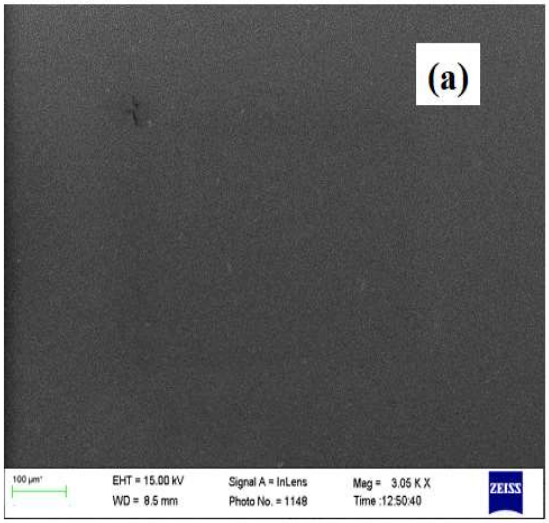
(a)
100 µm
EHT = 15.00 kV
WD = 8.5 mm
Signal A = InLens
Photo No. = 1148
Mag = 3.05 K X
Time :12:50:40
ZEISS

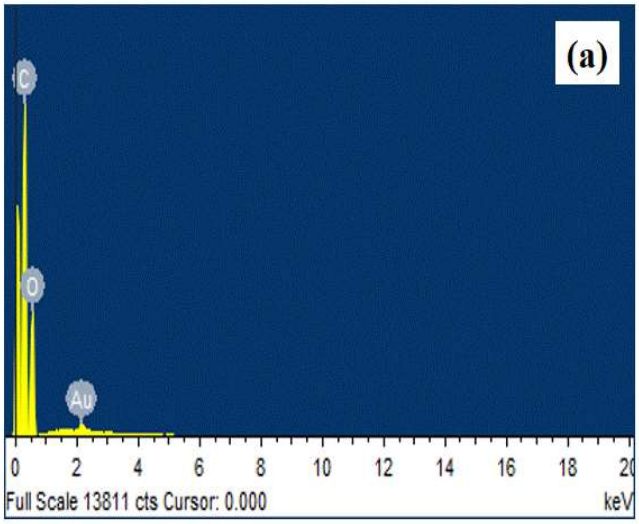
(a)
C
O
Au
0 2 4 6 8 10 12 14 16 18 20
Full Scale 13811 cts Cursor: 0.000
keV

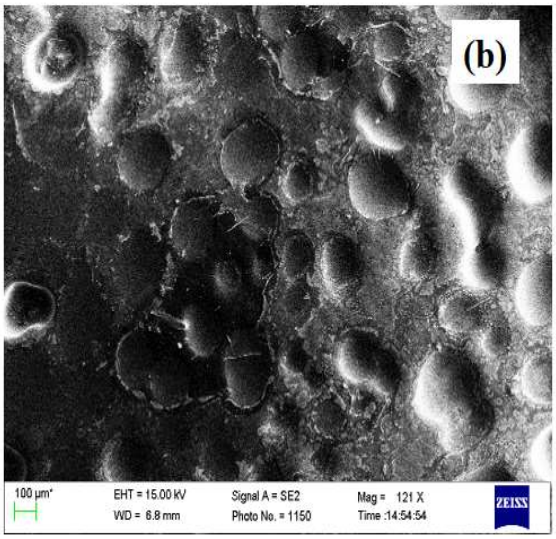
(b)
100 µm
EHT = 15.00 kV
WD = 6.8 mm
Signal A = SE2
Photo No. = 1150
Mag = 121 X
Time :14:54:54
ZEISS

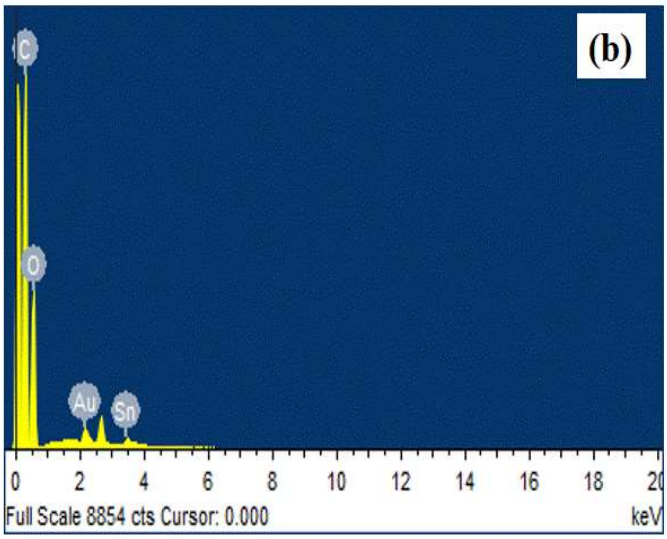
(b)
C
O
Au
Sn
0 2 4 6 8 10 12 14 16 18 20
Full Scale 8854 cts Cursor: 0.000
keV

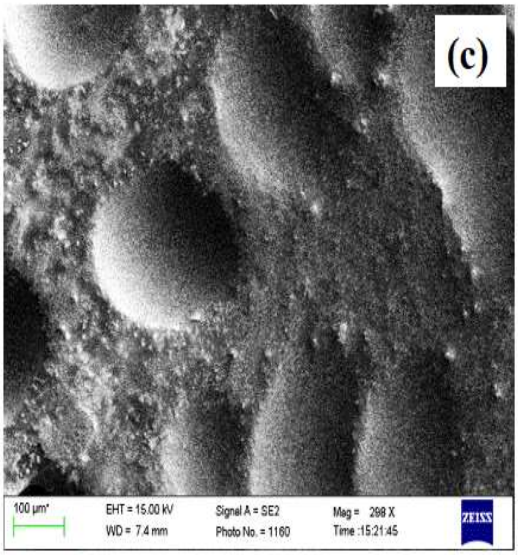
(c)
100 µm
EHT = 15.00 kV
WD = 7.4 mm
Signal A = SE2
Photo No. = 1160
Mag = 298 X
Time :15:21:45
ZEISS

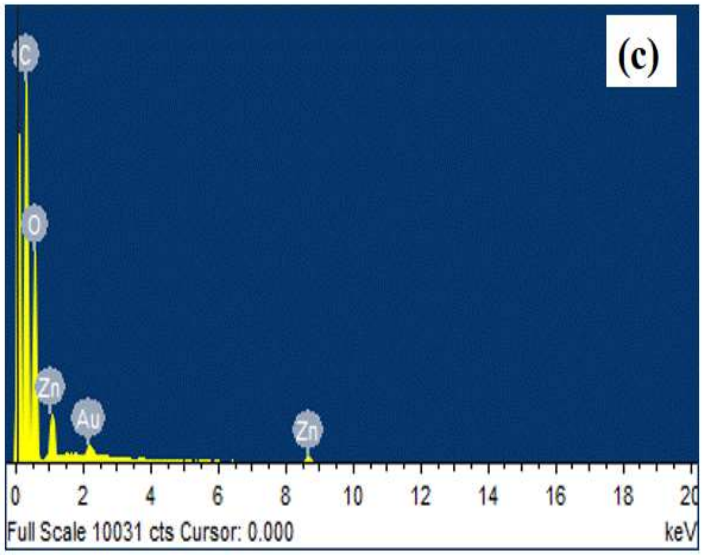
(c)
C
O
Zn
Au
Zn
0 2 4 6 8 10 12 14 16 18 20
Full Scale 10031 cts Cursor: 0.000
keV

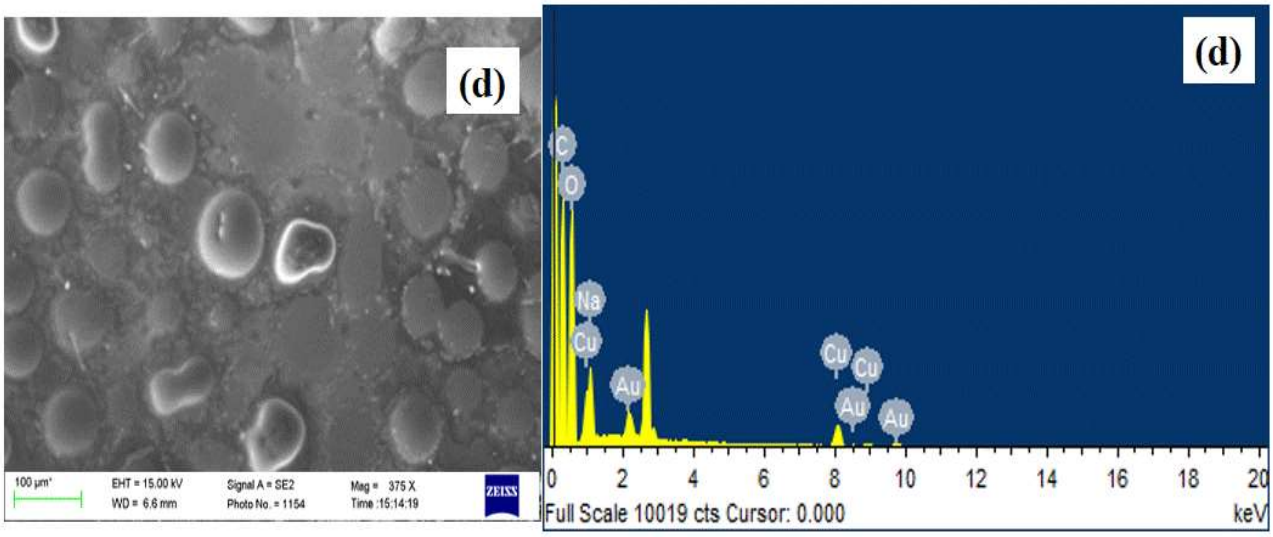

Fig. 5.3 SEM-EDS images of a) PGS b) PGS-SnO c) PGS-ZnO d) PGS-CuO

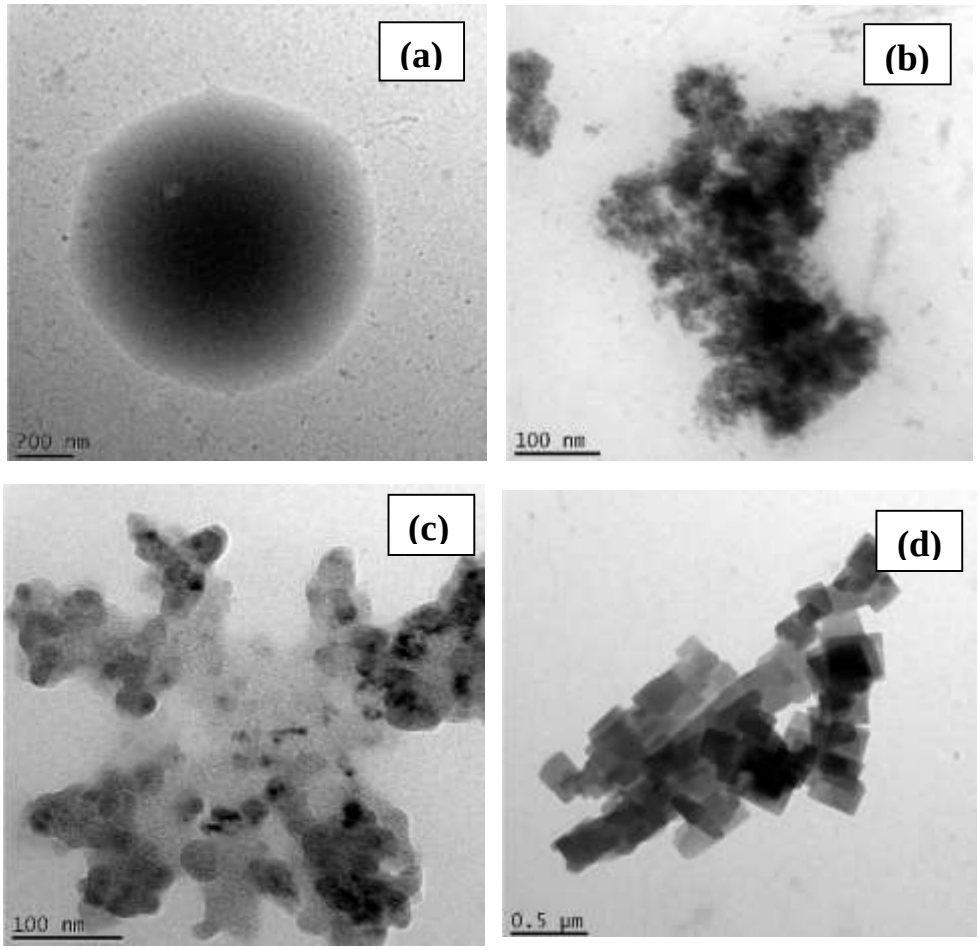

Fig. 5.4 TEM images of a) PGS b) PGS-SnO c) PGS-ZnO d) PGS-CuO

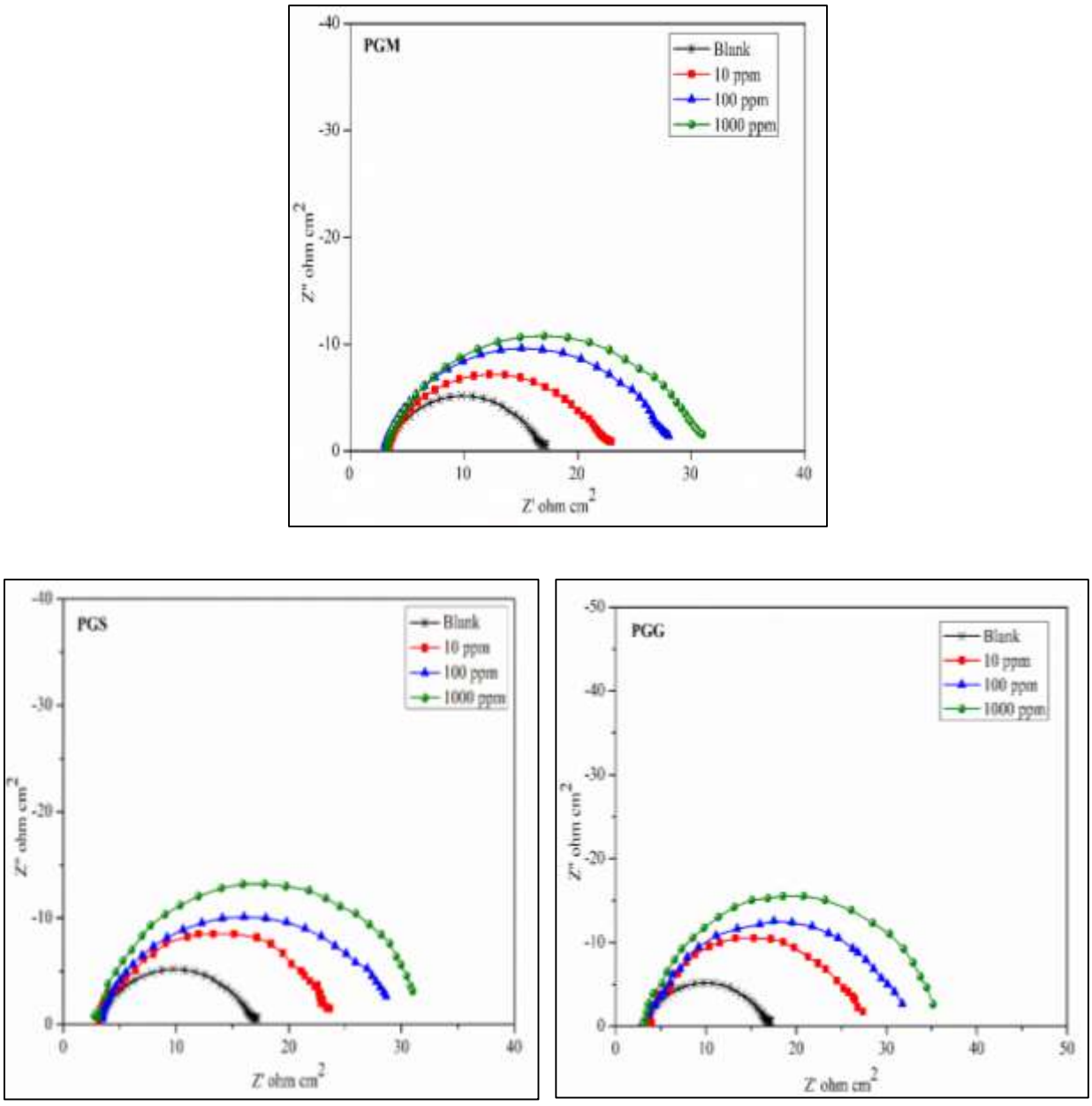

Fig. 5.5 Nyquist plots of parent precursors for corrosion of mild steel in 0.5 M H_2SO_4

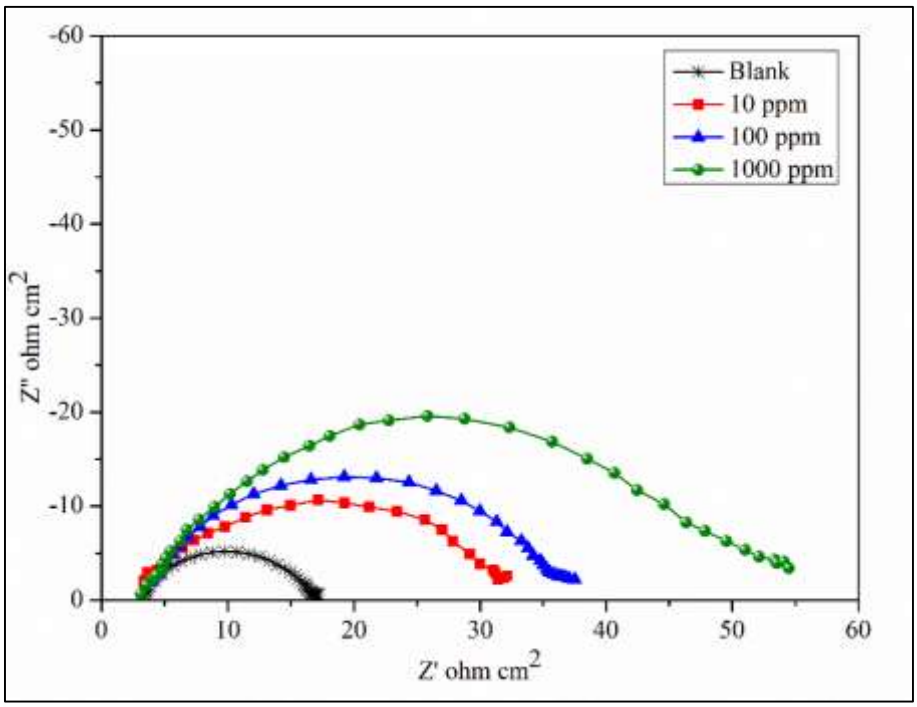

Fig. 5.6(a) Nyquist representation of PGM-SnO NPs for the corrosion of mild steel in 0.5 M H_2SO_4

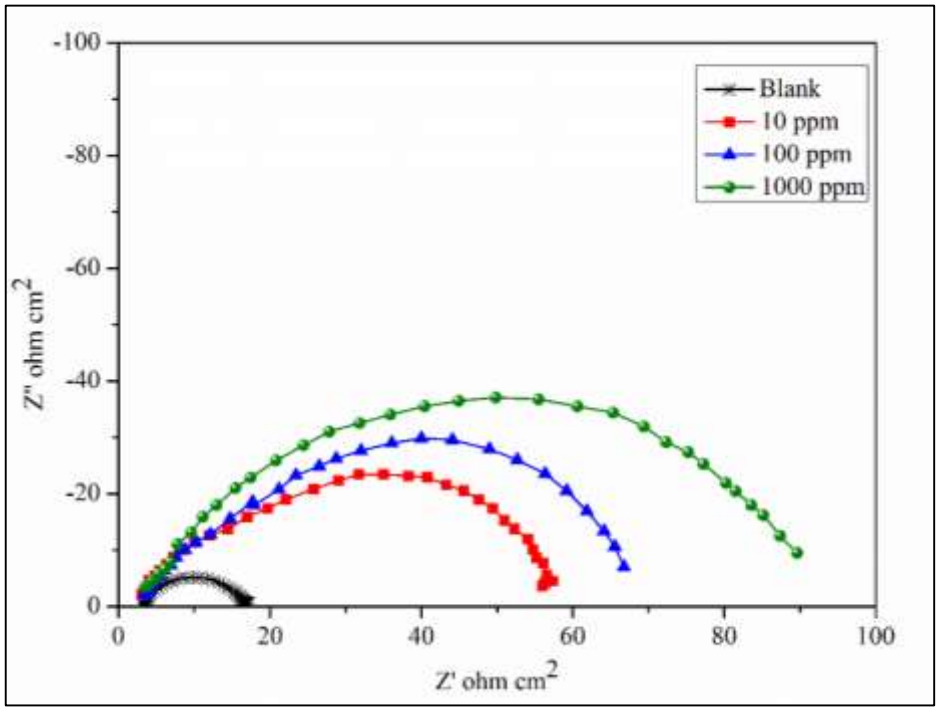

Fig. 5.6(b) Nyquist representation of PGM-ZnO NPs for the corrosion of mild steel in 0.5 M H_2SO_4

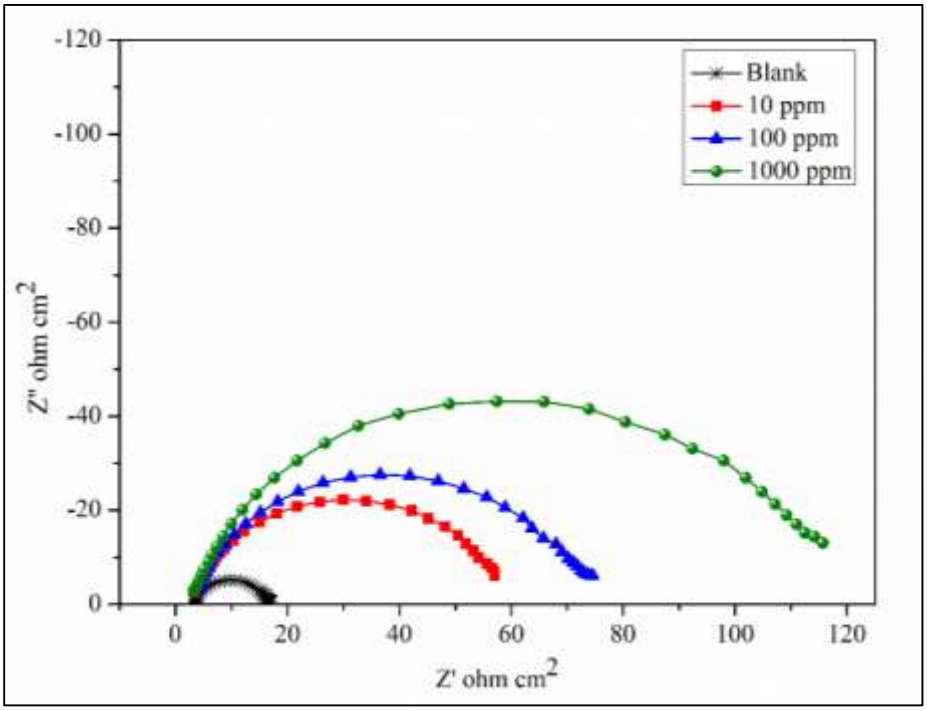

Fig. 5.6(c) Nyquist representation of PGM-CuO NPs for the corrosion of mild steel in 0.5 M H_2SO_4

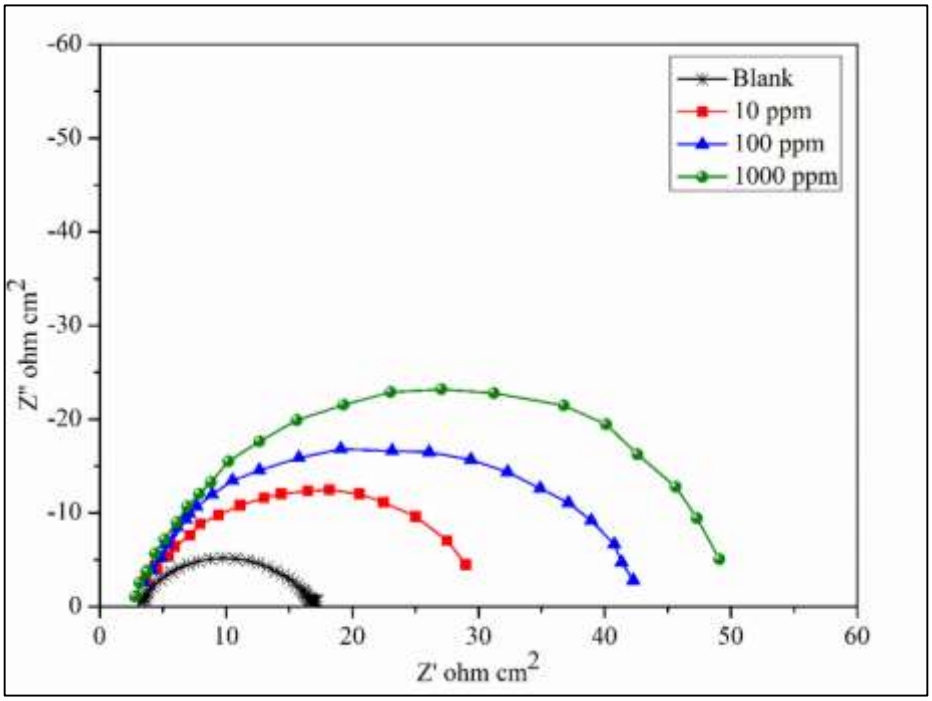

Fig. 5.6(d) Nyquist representation of PGS-SnO NPs for the corrosion of mild steel in 0.5 M H_2SO_4

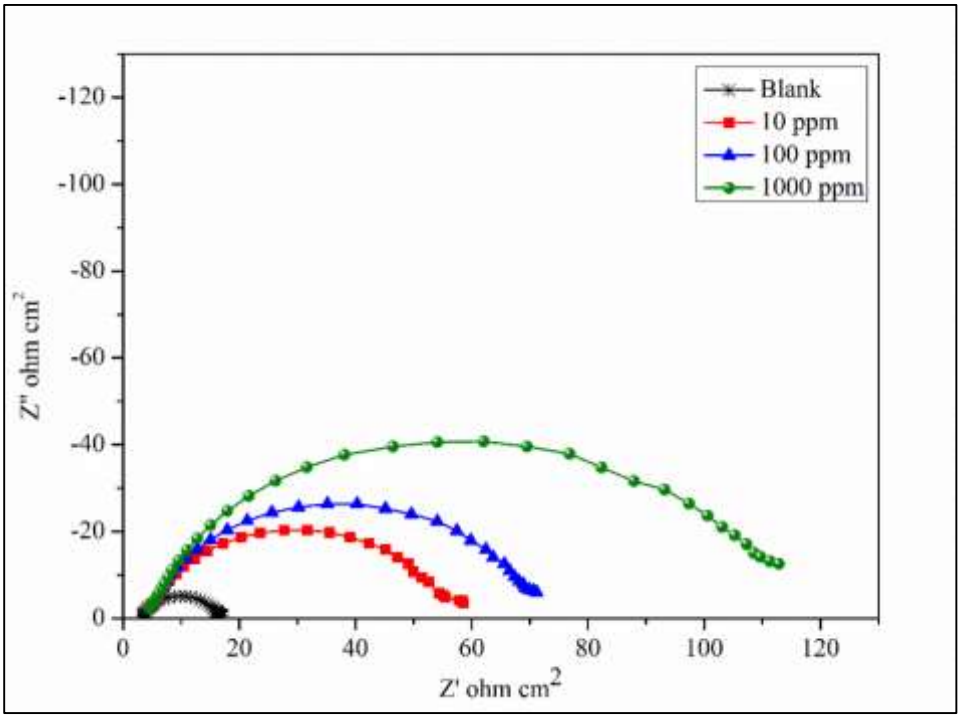

Fig. 5.6(e) Nyquist representation of PGS-ZnO NPs for the corrosion of mild steel in 0.5 M H_2SO_4

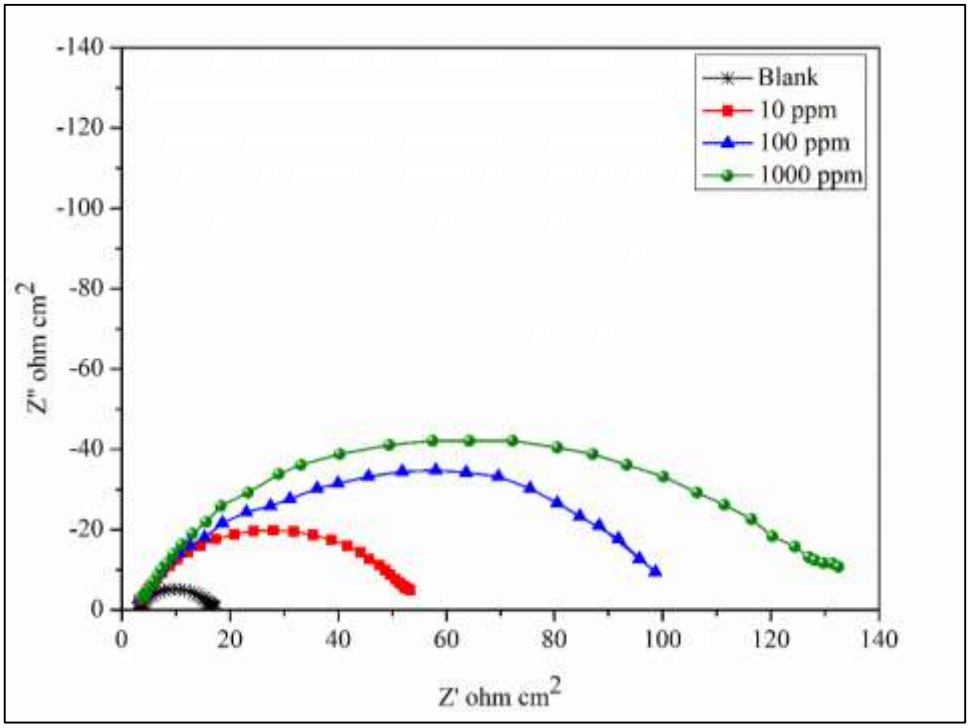

Fig. 5.6(f) Nyquist representation of PGS-CuO NPs for the corrosion of mild steel in 0.5 M H_2SO_4

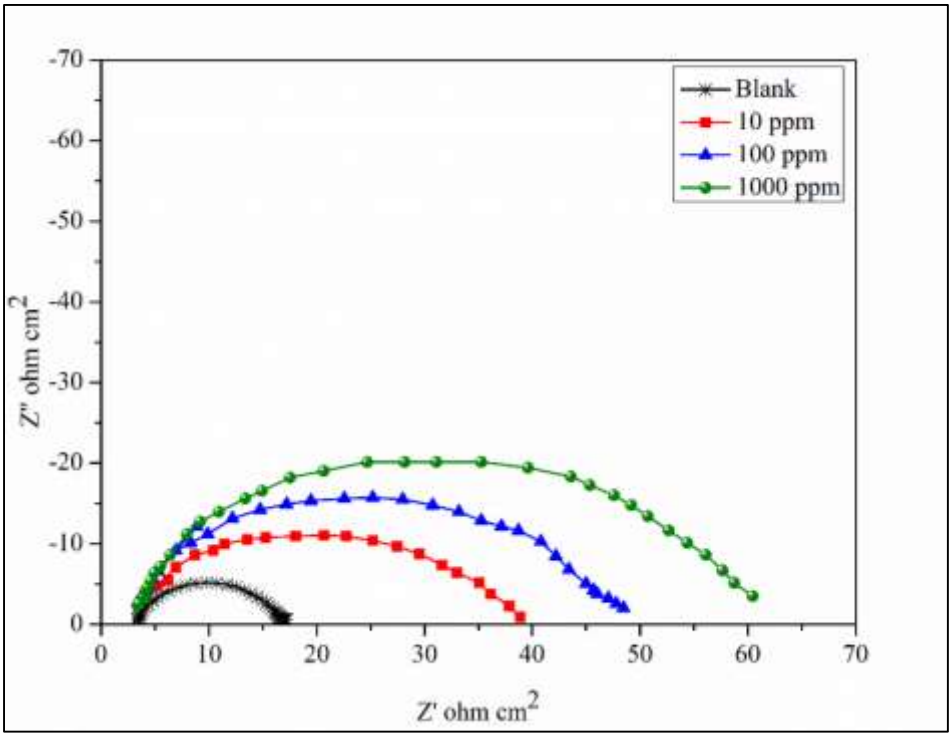

Fig. 5.6(g) Nyquist representation of PGG-SnO NPs for the corrosion of mild steel in 0.5 M H_2SO_4

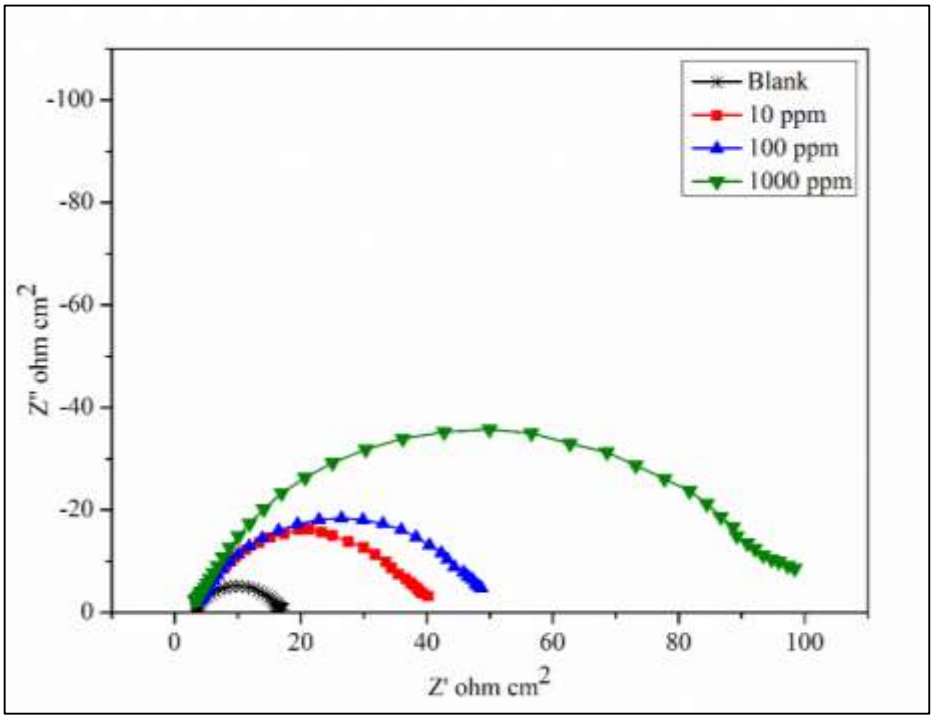

Fig. 5.6(h) Nyquist representation of PGG-ZnO NPs for the corrosion of mild steel in 0.5 M H_2SO_4

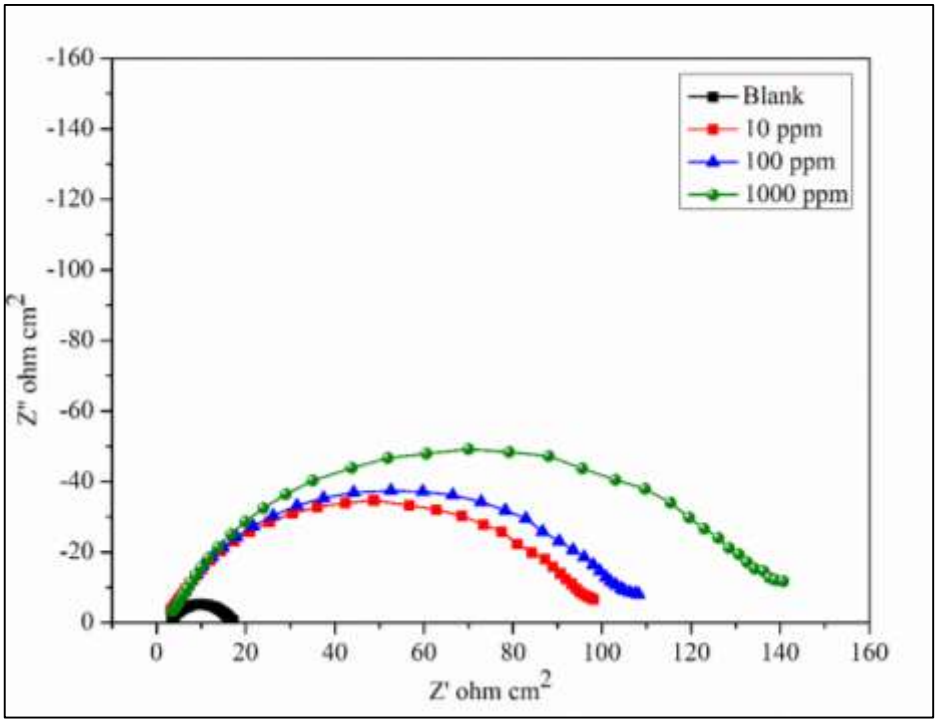

Fig. 5.6(i) Nyquist representation of PGG-CuO NPs for the corrosion of mild steel in 0.5 M H_2SO_4

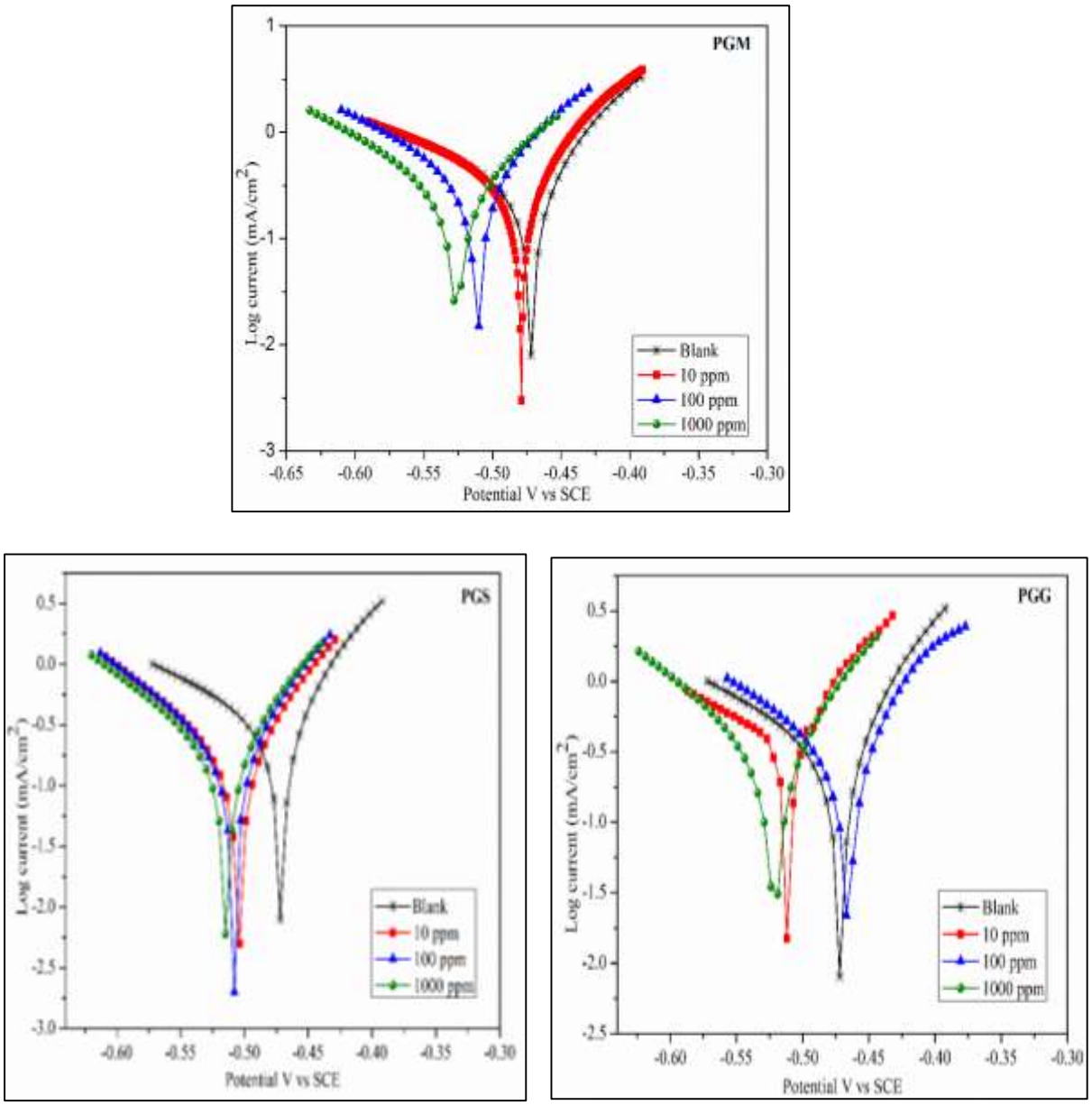

Fig. 5.7 Tafel plots of parent precursors for the corrosion of mild steel in 0.5 M H_2SO_4

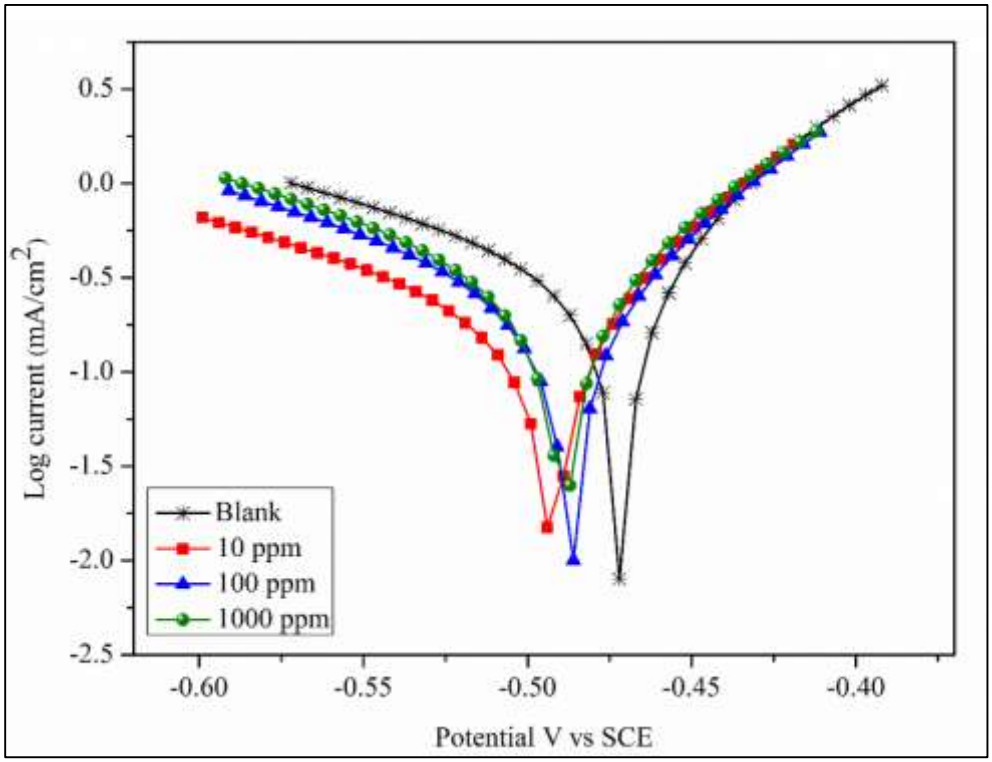

Fig. 5.8(a) Tafel plot of PGM-SnO NPs for the corrosion of mild steel in 0.5 M H_2SO_4

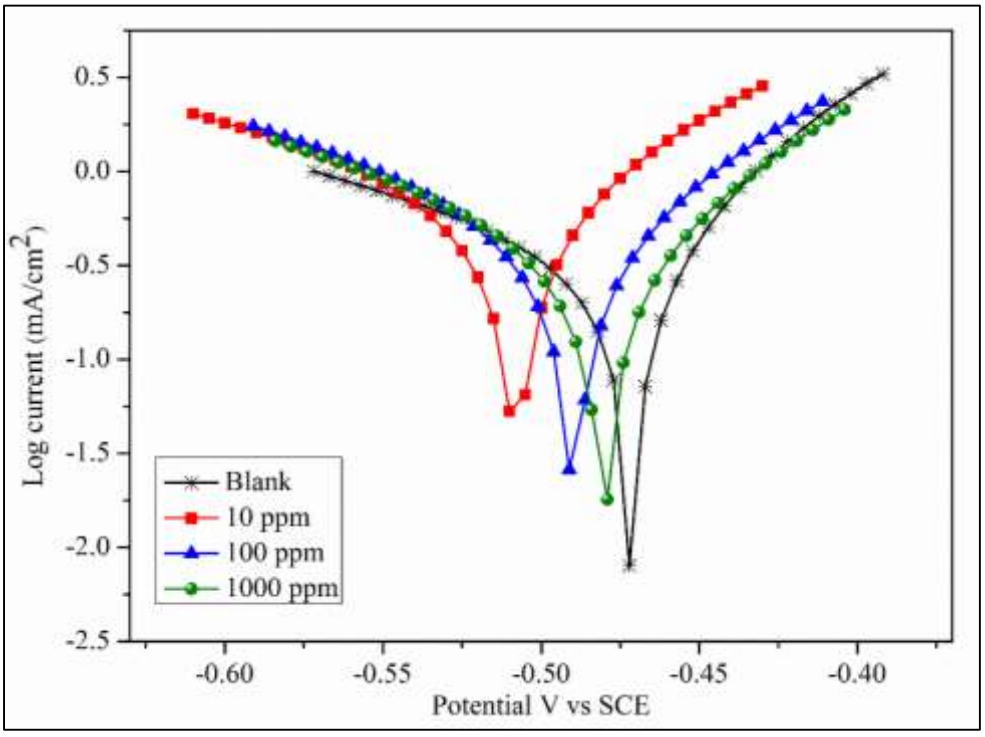

Fig. 5.8(b) Tafel plot of PGM-ZnO NPs for the corrosion of mild steel in 0.5 M H_2SO_4

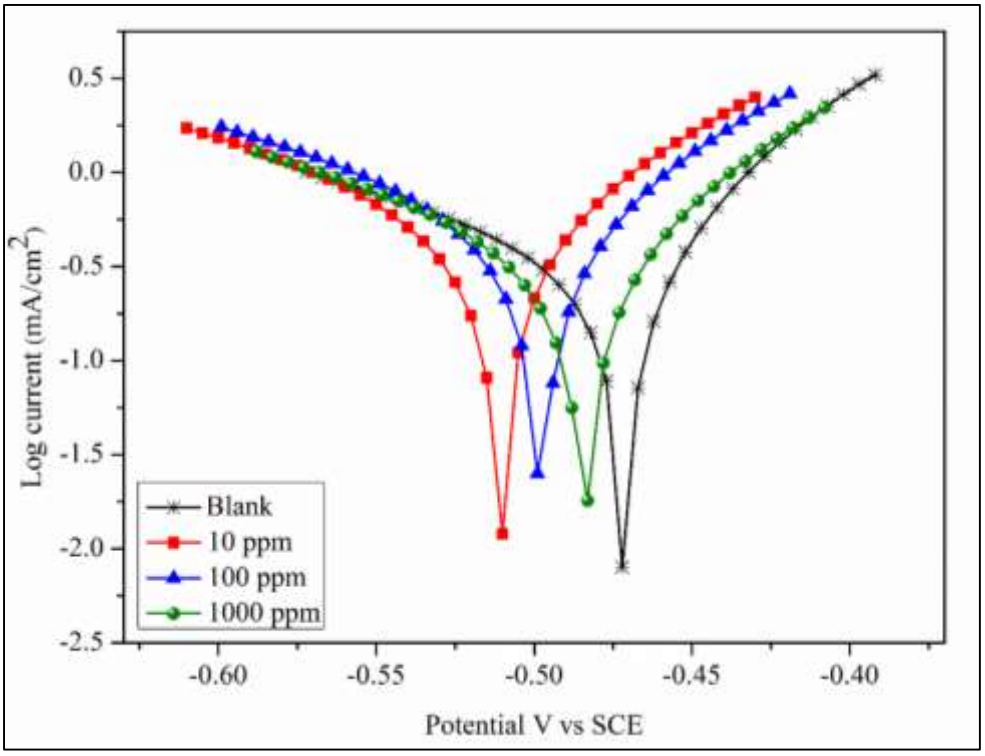

Fig. 5.8(c) Tafel plot of PGM-CuO NPsfor the corrosion of mild steel in 0.5 M H_2SO_4

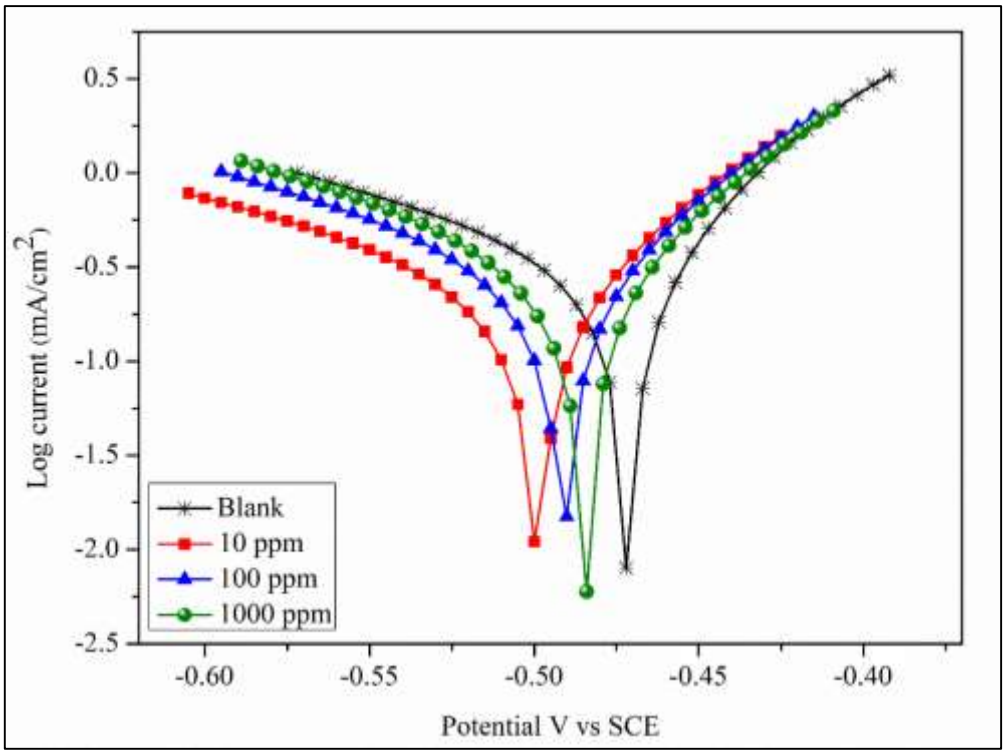

Fig. 5.8(d) Tafel plot of PGS-SnO NPs for the corrosion of mild steel in 0.5 M H_2SO_4

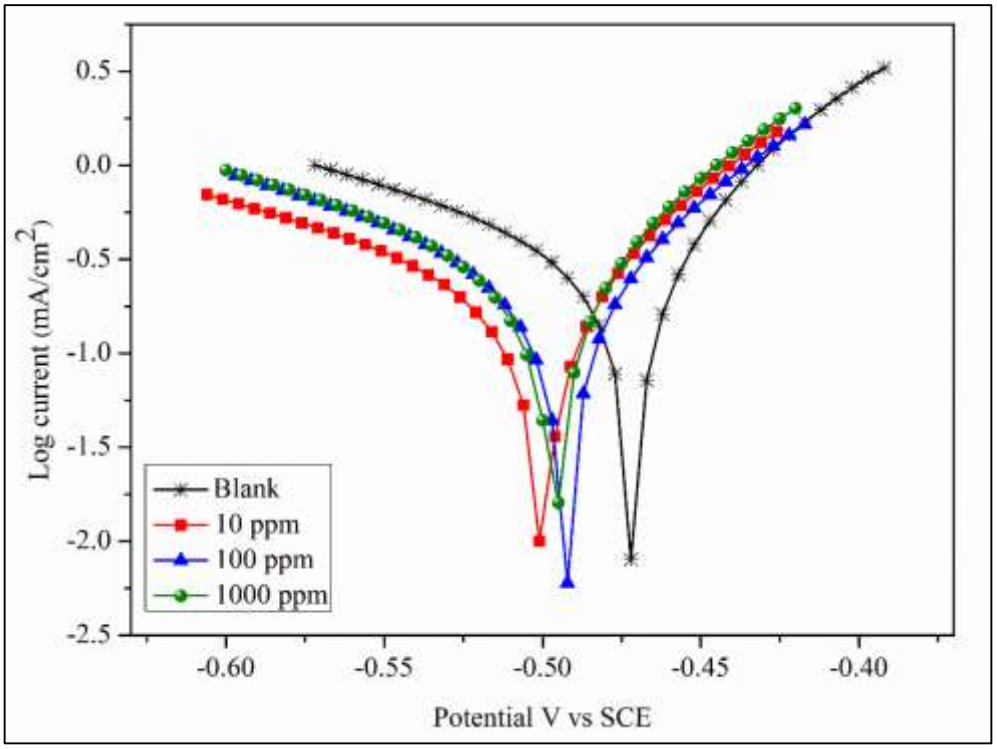

Fig. 5.8(e) Tafel plot of PGS-ZnO NPs for the corrosion of mild steel in 0.5 M H_2SO_4

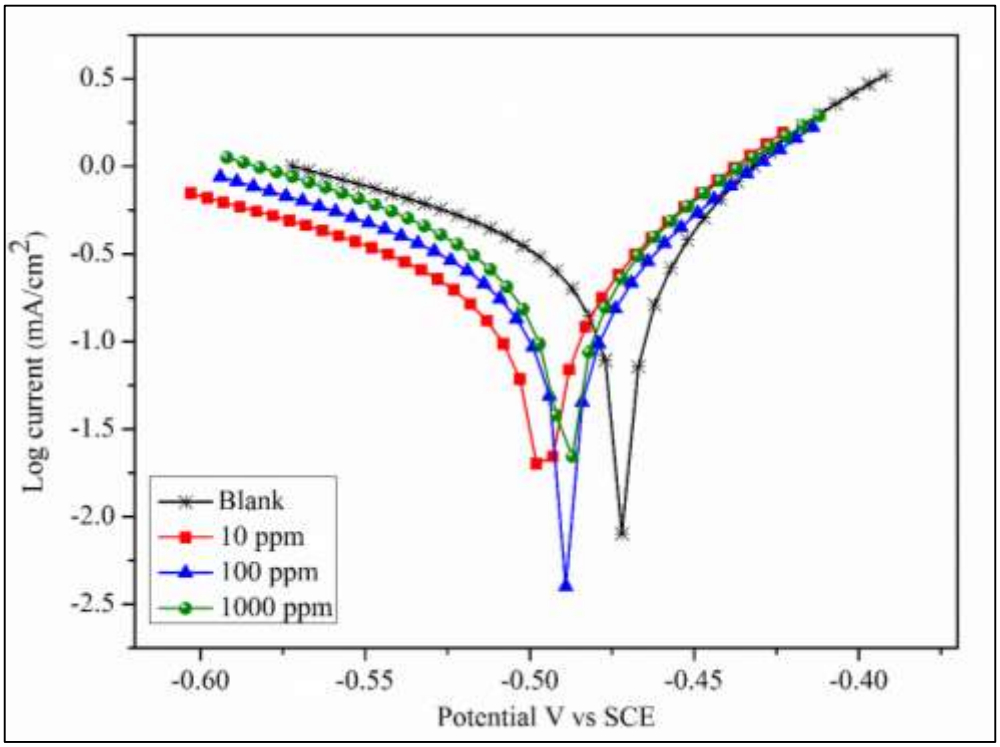

Fig. 5.8(f) Tafel plot of PGS-CuO NPs for the corrosion of mild steel in 0.5 M H_2SO_4

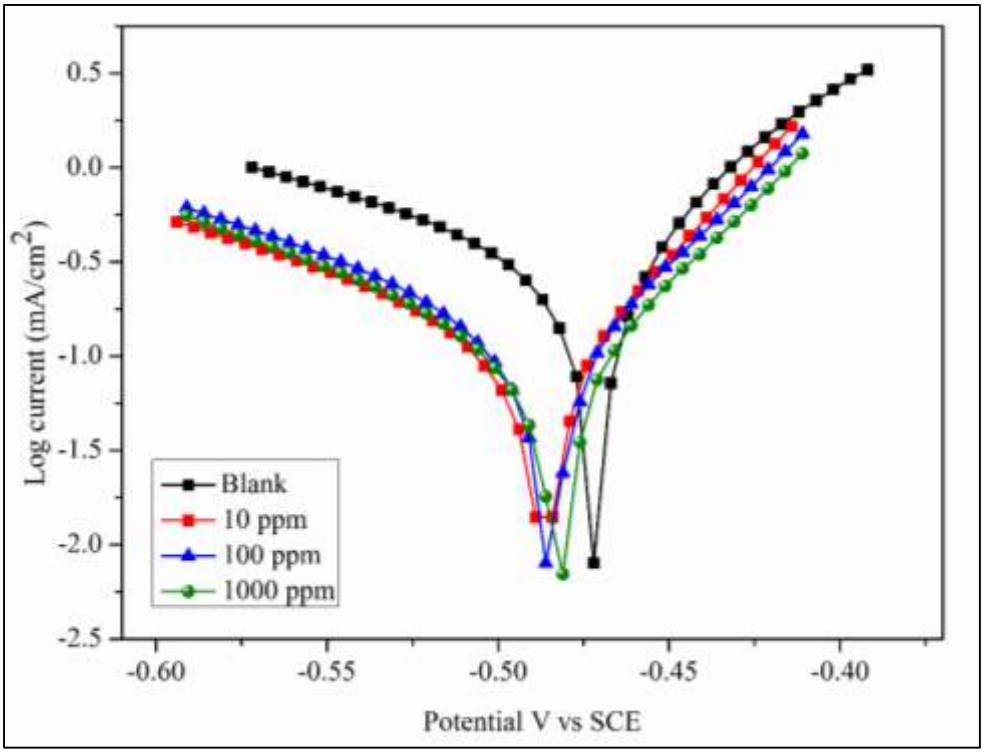

Fig. 5.8(g) Tafel plot of PGG-SnO NPs for the corrosion of mild steel in 0.5 M H_2SO_4

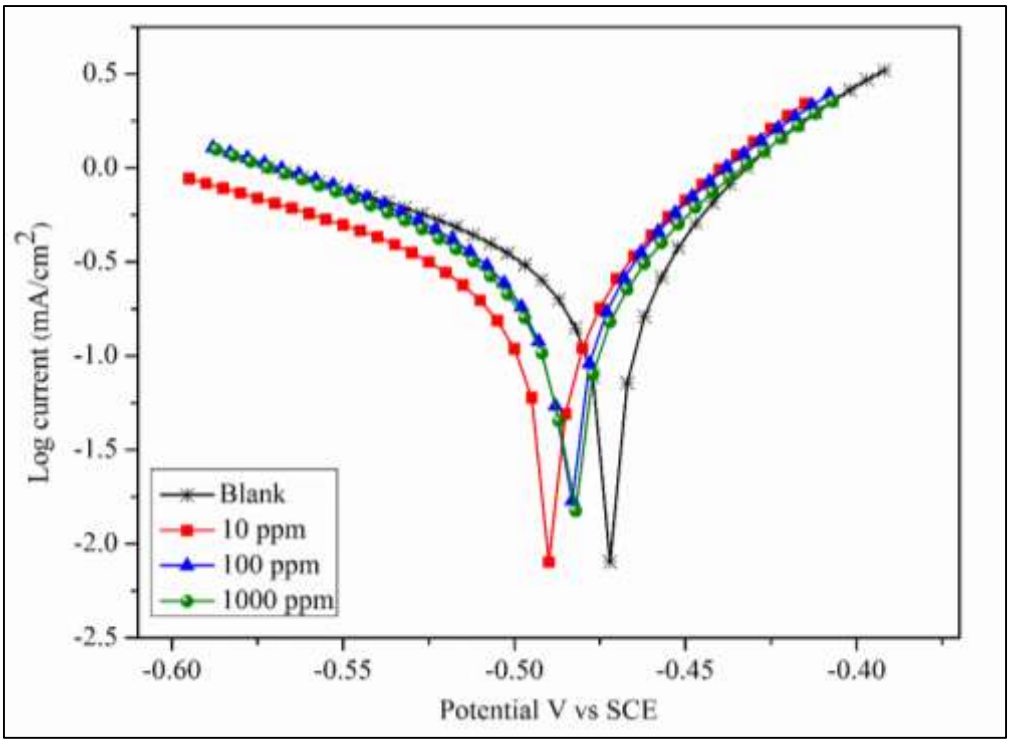

Fig. 5.8(h) Tafel plot of PGG-ZnO NPs for the corrosion of mild steel in 0.5 M H_2SO_4

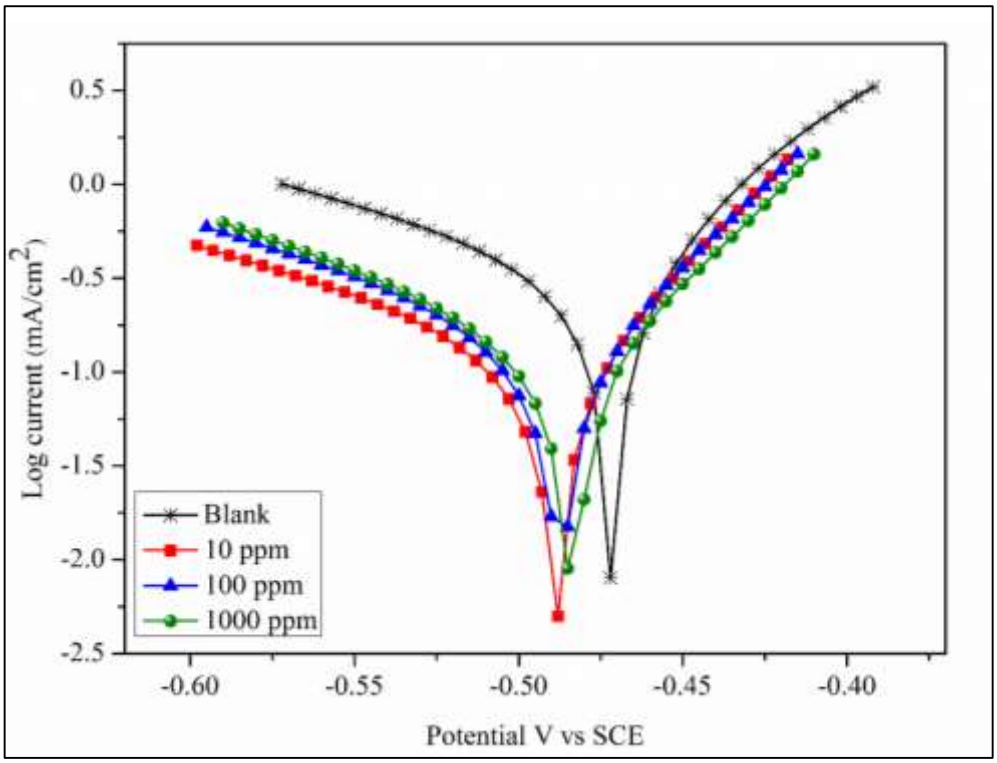

Fig. 5.8(i) Tafel plot of PGG-CuO NPs for the corrosion of mild steel in 0.5 M H_2SO_4

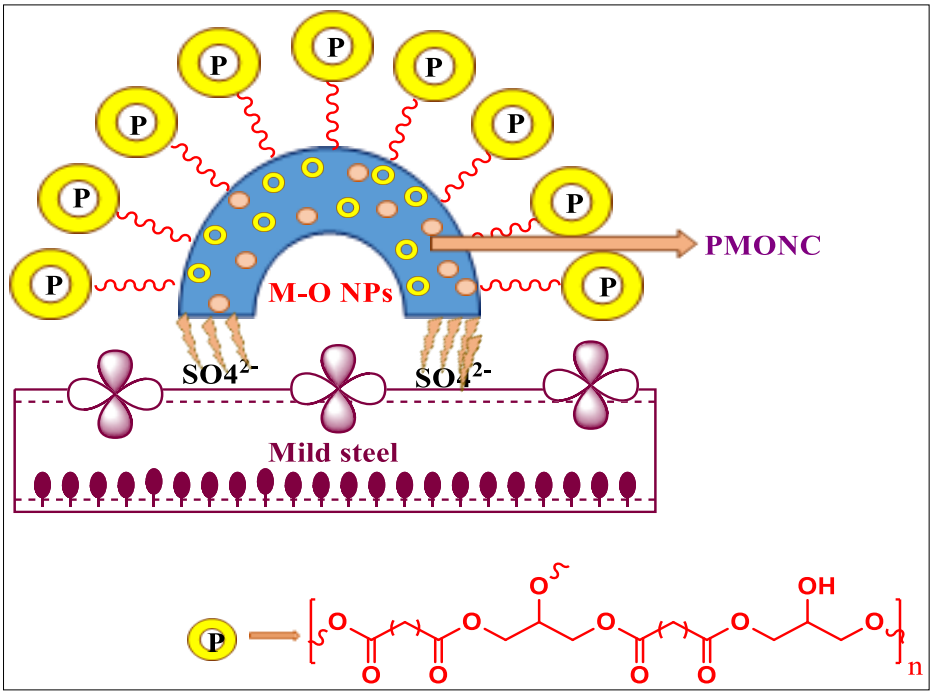

Fig. 5.9 Proposed corrosion mitigation mechanism